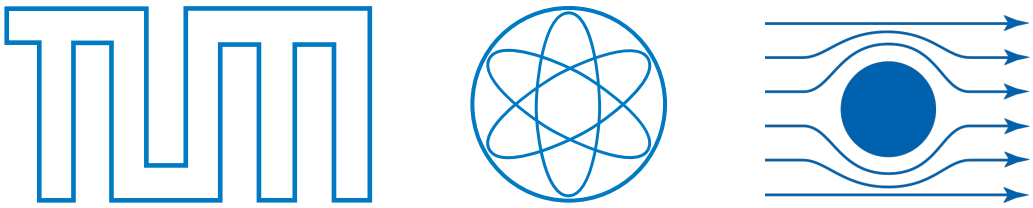

Technische Universität München
Fakultät für Physik
Walther-Meißner-Institut für Tieftemperaturforschung

Bachelor's Thesis in Physics

Hall Effect Measurements in YIG/Pt hybrids

Richard Schlitz

Garching, August 9, 2013

Supervisor: Dr. Sebastian T. B. Goennenwein

First reviewer (Supervisor): Dr. Sebastian T. B. Goennenwein

Second reviewer: Prof. Dr. Christian Pfleiderer

Contents

1 Introduction 1

2 Theoretical Background 3
2.1 Spin Currents 3
2.2 Spin Hall Effect 4
2.3 Spin Hall Magnetoresistance 5
2.4 Ordinary and Extraordinary Hall Effect 7
2.5 Spin Hall AHE 8

3 Experimental Methods and Setup 11
3.1 Sample Preparation 11
3.2 Magnet Setup 12
3.2.1 Room Temperature Electromagnet 12
3.2.2 Magnet Cryostat 13
3.3 Measurement Techniques 14

4 Results and Discussion 15
4.1 Magnetization in Thin Ferromagnetic Films 15
4.2 Thickness dependece of ρ_0 18
4.3 Ordinary Hall Coefficient 19
4.4 Anomalous Hall Effect 29

5 Conclusions and Outlook 37

A Symmetrization with PYTHON 41

B Used Samples 45

Bibliography 50

Acknowledgements 51

Chapter 1

Introduction

In 1879, Edwin Hall discovered the "Hall" effect during his PhD thesis [1]. He put thin gold foil ($t_{\mathrm{Au}} \sim 1\,\mu\mathrm{m}$) into a magnetic field, drove a current through it and observed an electric potential V_{trans} perpendicular to the applied current, when the magnetic field vector is pointing perpendicular to the film plane. Though searched for, if it would not have been for the thin film ($V_{\mathrm{trans}} \sim \frac{1}{t_{\mathrm{Au}}}$), the effect would probably not have been discovered so early, as the measurement equipment at that time had a lower sensitivity than today.

Two years later, in 1881, Edwin Hall also discovered the anomalous Hall effect in nickel, cobalt and iron, resulting from the magnetization within these materials [2]. The anomalous Hall effect can have a much larger magnitude than the ordinary Hall effect and is by now, 130 years later, still not totally understood in ferromagnetic materials, as it is hard to explain in its entirity [3–5].

In a non-magnetic normal metal, e.g. platinum, no anomalous Hall effect is expected. Even in close proximity to a ferromagnetic insulator, no induced magnetic moments are observed [6]. Thus, in the case of a ferromagnetic insulator/normal metal hybrid structure, no anomalous Hall effect is anticipated.

As data storage, currently based on charge, is reaching its physical limits, the additional degree of freedom of electrons, the spin angular momentum or "spin" can be used to enhance the current devices. To utilize spin, one needs to be able to generate, manipulate and implement it to the current technology. The spin Hall effect [7–9] allows to electronically generate spin currents in materials with large spin orbit coupling [10]. Therefore, normal metals can be used as "spin sources". Even if its name suggests an analogy to the well known Hall effect, this analogy fails, as the spin current is generated by the the spin Hall effect due to spin dependent scattering, even in the absence of a magnetic field [7, 10]. The inverse spin Hall effect [11], transforming spin currents to charge currents, can be utilized to build a device, too, that can act as a spin detector.

The recently discovered spin Hall magnetoresistance (SMR) [12, 13] in normal

metal/ferromagnetic insulator hybrid structures, is exactly the combination of these effects. The SMR effect was observed as a change of resistivity during rotations of the hybrid structures in a fixed magnetic field and magnetic field sweeps and thus is a magnetoresistance effect.

The SMR effect allows to extract the material properties of a normal metal, relevant to spin dependent transport experiments, as it has been already done for platinum [13]. Like Edwin Hall's ordinary Hall effect, this effect can only be observed for very low thicknesses, as its relative magnitude is very small for high thicknesses. The spin transport parameters are "need to know", if one wants to utilize spin dependent transport, for example in spintronics, where not charge is used as binary "1" and "0" but "spin up" and "spin down" as "1" and "0". By utilizing the SMR effect, one can parametrize devices to use as spin valves or spin transistors [14].

Thus, this kind of hybrid structure "device" was subject to investigations during this thesis, as Y. T. Chen [15] proposed an additional effect, the spin Hall anomalous Hall effect in platinum, for yttrium iron garnet/platinum hybrid structures. However, in the course of this thesis it was necessary to obtain the ordinary Hall coefficient A_{OHE} of the platinum thin films, as $A_{\mathrm{OHE}}(t_{\mathrm{Pt}})$ needs to be known to seperate the contributions of the proposed anomalous Hall effect. As a result of these experiments, it was discovered, that the ordinary Hall coefficient for low platinum thicknesses is significantly changed by so far unknown effects. Therefore, even after more than 130 years, the ordinary Hall coefficient still offers avenues to new physics.

This thesis is split into five chapters. In the following Ch. 2, the necessary theoretical background is presented and relevant diagrams are shown. Chapter 3 gives a short overview of the sample preparation, the used setups and the measurement techniques used during this thesis. The results of the measurements in the different setups will be presented, compared and discussed in Ch. 4. Concluding this thesis, a short summary is given and suggestions for future experiments are outlined in Ch. 5.

Chapter 2

Theoretical Background

The Spin Hall Magnetoresistance (SMR) [12,13,15] is caused by the simultaneous action of the spin Hall effect (SHE) [7–9] and the inverse spin Hall effect (ISHE) [11]. All these mechanisms are to be discussed in this chapter. We furthermore will illuminate spin currents, the ordinary and extraordinary Hall effects [1–5], the spin Hall anomalous Hall effect [15] will conclude this chapter.

2.1 Spin Currents

A charge current in a metal is carried by electrons. These have an additional degree of freedom, the spin angular momentum or spin. The projection of the spin vector $\hat{\mathbf{s}}$ can either be pointing parallel or antiparallel to the quantization axis $\hat{\mathbf{z}}$ [16]. These two states are called "spin up" for $\hat{\mathbf{s}} \uparrow\uparrow \hat{\mathbf{z}}$ and "spin down" for $\hat{\mathbf{s}} \downarrow\uparrow \hat{\mathbf{z}}$.

The only property of an electron relevant to a charge current is the charge $q = -e$. Hence, as the charge current is independent of the electron spin, one can express the charge current $\mathbf{J}_\mathrm{q}$ as

$$\mathbf{J}_\mathrm{q} = \mathbf{J}_\uparrow + \mathbf{J}_\downarrow. \tag{2.1}$$

The total charge current is therefore the sum of the charge current carried by spin up electrons $\mathbf{J}_\uparrow$ and spin down electrons $\mathbf{J}_\downarrow$. As long as there is no spin dependent scattering, and the system is in equlibrium, one can assume, that the contributions of electrons with spin up and spin down are equal ($\mathbf{J}_\uparrow = \mathbf{J}_\downarrow$), as the spin is uniformly distributed among the electrons. The conductivities for electrons with spin up and spin down are equal ($\sigma_\uparrow = \sigma_\downarrow = \sigma$). This is sktched in Fig. 2.1 (a).

Assuming there are mechanisms changing the conductivity for electrons with either spin direction ($\sigma_\uparrow \neq \sigma_\downarrow$), an imbalance between the two contributions to the charge current is created and therefore it is accompanied by a spin current [17]

$$\mathbf{J}_\mathrm{s} = -\frac{\hbar}{2e}(\mathbf{J}_\uparrow - \mathbf{J}_\downarrow). \tag{2.2}$$

This so called spin polarized current is shown in Fig. 2.1 (b).

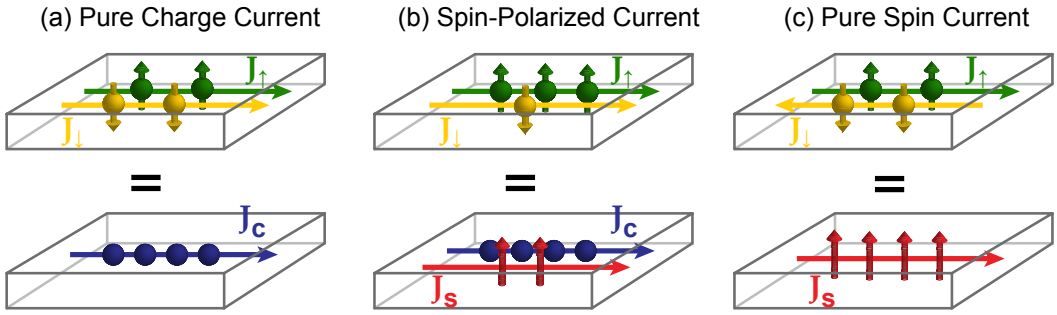

Figure 2.1: (a) Pure charge current. (b) Spin polarized current. (c) pure spin current. Illustration taken from [17].

Concluding this discussion, one can imagine spin up electrons flowing left and spin down electrons flowing right. This would result in a pure spin current which is depicted in Fig. 2.1 (c). The generation of spin polarized currents and pure spin currents in paramagnetic metals stems from spin dependent scattering effects due to the spin orbit coupling and can be explained in terms of extrinsic effects (side jump [18] and skew scattering [19]) and intrinsic effects. These intrinsic effects, dependent only on the band structure of the material, can be described in the context of the Berry phase [4]. For further information on this topic see [5].

2.2 Spin Hall Effect

As proposed by M. I. Dyakonov, V. I. Perel and J. E. Hirsch [7, 20], a charge current $\mathbf{J}_\mathrm{q}$ generates a spin current $\mathbf{J}_\mathrm{s}$

$$\mathbf{J}_\mathrm{s} = \Theta_\mathrm{SH} \left(-\frac{\hbar}{2e} \right) \mathbf{J}_\mathrm{q} \times \mathbf{s} \tag{2.3}$$

perpendicular to $\mathbf{J}_\mathrm{q}$ and the spin polarization $\mathbf{s}$ of the charge current. The effect is depicted in Fig. 2.2 (a). This so called spin Hall effect (SHE) arises due to spin orbit coupling of the electrons, making the scattering spin dependent and thus creating a spin current.

Equation (2.3) describes the generation of spin current due to the SHE [21]. The spin Hall angle Θ_SH is a material parameter reflecting the effectiveness in converting charge to spin currents. Metals with large spin orbit coupling like platinum show a spin Hall angle of $\Theta_\mathrm{Pt} \approx 0.1$ [13], whereas gold has a spin Hall angle of $\Theta_\mathrm{Au} \approx 0.022$ [22].

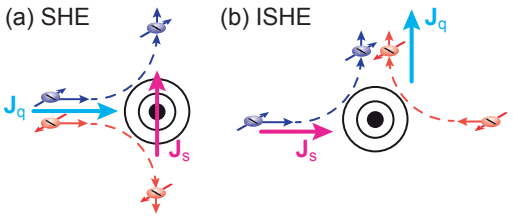

Figure 2.2: (a) Spin Hall effect: A pure charge current induces a perpendicular spin current. (b) Inverse spin Hall effect: A pure spin current induces a perpendicular charge current. The blue and red dashed arrows represent the trajectories of spin up and spin down electrons, respectively. Illustrations taken from [23].

The spin Hall angle can also be expressed as the fraction of spin conductivity σ_{spin} and electical conductivity σ_{el} [21]

$$\Theta_{\text{SH}} = \frac{\sigma_{\text{spin}}}{\sigma_{\text{el}}}. \tag{2.4}$$

The inverse spin Hall effect (ISHE) follows the same principle and is displayed in Fig. 2.2 (b). Now, a spin current generates a charge current perpendicular to both spin current direction and spin polarization due to the same scattering effects.

2.3 Spin Hall Magnetoresistance

Let us now assume a thin film of a nonmagnetic metal (NM), like platinum. An initial charge current $\mathbf{J}_{\text{q}}$ produces a perpendicular spin current by the action of the SHE. This leads to a spin accumulation at the interfaces of the normal metal. Following the gradient of the spin chemical potential, a spin diffusion current $\mathbf{J}_{\text{diff}}$ emerges, compensating the initial spin current. With the ISHE acting on this diffusion current, an additional charge current parallel to $\mathbf{J}_{\text{q}}$ is generated. Thus, the resisitivity of the metal in equilibrium remains unchanged.

By adding a ferromagnetic insulator (FMI) to the platinum at one interface, the boundary conditions are redefined since a spin current is able to enter the FMI via spin transfer torque [15] if the magnetization $\mathbf{M}$ of the FMI points in the right direction. This transfer of spin angular momentum is furthermore governed by the spin mixing interface conductance $G_{\uparrow\downarrow} = G_{\text{r}} + iG_{\text{i}}$. The real part G_{r} dominates this term and can be pictured as resistivity for the spin current flow through the interface [24], whereas the imaginary part G_{i} can be "interpreted as an effective exchange field acting on the spin accumulation" [15] and gives rise to the spin Hall anomalous Hall effect (c.f. Sec. 2.5).

The spin transfer torque is only transferrable, if the magnetization vector $\mathbf{M}$ has a component $\mathbf{M}_{\perp} \perp \mathbf{s}$ [15,24]. One can easily imagine this, as no angular momentum can be transferred when the magnetization is parallel to the spin polarization. If there is a perpendicular component, angular momentum can be transferred and the

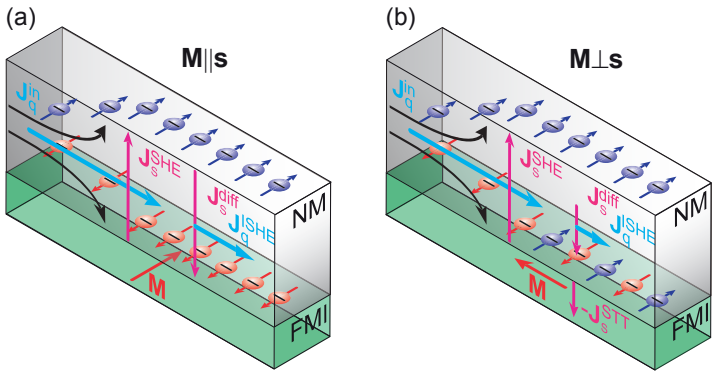

Figure 2.3: Sketch of the combined action of the spin Hall effect and the inverse spin Hall effect in a ferromagnetic insulator (FMI)/normal metal (NM) hybrid structure. (a) For $M \parallel s$, there is no spin current entering the FMI. (b) For $M \perp s$, the spin current excites a spin transfer torque in the FMI and thus the resistance is increased. Illustration taken from [23].

magnetization vector $\mathbf{M}$ in the ferromagnetic layer starts a precession around its original direction.

If there is no component of $\mathbf{M} \perp \mathbf{s}$, the spin current is totally reflected at the interface between the FMI and the NM. Otherwise, if there is a component $\mathbf{M} \perp \mathbf{s}$, it is possible for the electrons at the interface to transfer spin angular momentum into the FMI and therefore loose their spin information. Resulting from this, the gradient of the spin chemical potential is reduced, decreasing the spin diffusion current $\mathbf{J}_\mathrm{s}^\mathrm{diff}$ and thus, also the charge current produced via the ISHE and thus increasing the resistance of the NM layer. The two limits of this consideration are shown in Fig. 2.3.

Starting from the spin diffusion equation for the NM layer, and assuming one interface with spin current flow (FMI/NM interface) depending on the magnetization orientation of the FMI, one obtains two equations, one for the dependence of the longitudinal specific resistance ρ_long and one for the dependence of the transverse specific resistance ρ_trans on the magnetization direction [15].

$$\rho_\mathrm{long} = \frac{V_\mathrm{long}}{I_\mathrm{q}} \frac{t_\mathrm{NM} w}{l} = \rho_0 + \rho_1 \mathbf{m}_\mathrm{t}^2 \tag{2.5}$$

$$\rho_\mathrm{trans} = \frac{V_\mathrm{trans}}{I_\mathrm{q}} t_\mathrm{NM} = \rho_2 \mathbf{m}_\mathrm{n} + \rho_3 \mathbf{m}_\mathrm{j} \mathbf{m}_\mathrm{t} \tag{2.6}$$

ρ_0 is the bulk resistivity of the normal metal, $\Delta\rho_1/\rho_0 = -\Delta\rho_3/\rho_0$ the direct SMR related change in resistivity and ρ_2 the Hall effect related resistivity including an additional contribution from the Spin Hall AHE discussed in Sec. 2.5. $\mathbf{m}_\mathrm{n}$, $\mathbf{m}_\mathrm{t}$ and

$\mathbf{m}_\mathrm{j}$ are the projections of the magnetization direction vector $\mathbf{m} = \frac{\mathbf{M}}{M_\mathrm{s}}$ in the normal direction $\mathbf{n}$, the transverse direction $\mathbf{t}$ and the current direction $\mathbf{j}$, respectively. The definition of the directions can be seen in Fig. 2.4.

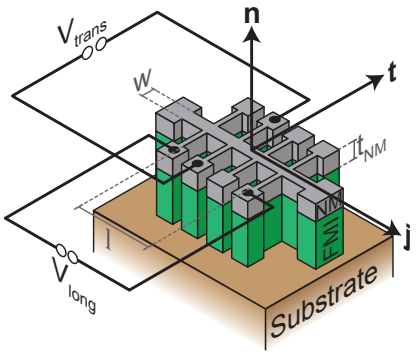

Figure 2.4: Sketch of the coordinate system and the sample structure. In analogy to [13].

As mentioned above, the increase of the longitudinal resistance due to the SMR only takes place if $\mathbf{M} \perp \mathbf{s}$. As only spin currents along the $\mathbf{n}$ direction are relevant to the SMR effect, the quantization axis of the spin polarization $\mathbf{s}$ is $\mathbf{t}$. So as $\mathbf{s} \parallel \mathbf{t}$, the (longitudinal) SMR is observed for non-vanishing components of $\mathbf{m}_\mathrm{t}$. It is thus possible to gradually change the resistance of the normal metal thin film by ρ_1 by rotating the magnetization of the FMI.

2.4 Ordinary and Extraordinary Hall Effect

The ordinary Hall effect(OHE) is a long known effect observed in conductors in an external magnetic field $\mathbf{H}$ and was first discovered by Edwin Hall in 1879 [1]. The charge carriers carrying the current I_q within the conductor are deflected by the Lorentz force and thus, if the charge carriers can accumulate at the interfaces (open boundary conditions), an electric field perpendicular to $\mathbf{H}$ and I_q is created. The measurement geometry to observe the effect is shown in Fig. 2.5.
One can derive

$$\rho_\mathrm{trans} = A_\mathrm{H} B \tag{2.7}$$

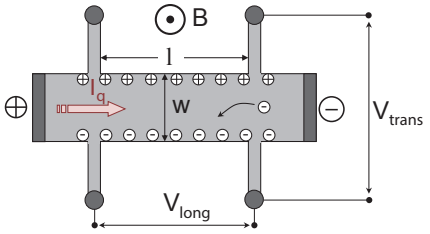

Figure 2.5: Geometry for measuring the ordinary Hall effect in a conducting film with thickness t. In analogy to [25].

for the transverse specific resistance using the Drude model [25]. Equation (2.7) shows a linear dependence of ρ_{trans} on the magnetic flux densitiy B and contains the Hall coefficient $A_{\text{H}} = \frac{1}{nq}$, with n being the free charge carrier density of the conducter and q the charge of the charge carriers.

Reformulating this in terms of the transverse resistance $R_{\text{trans}} = \frac{V_{\text{trans}}}{I_{\text{q}}}$, one obtains the following equation for the ordinary Hall coefficient

$$A_{\text{H}} = \frac{R_{\text{trans}} t}{B} \text{ with } R_{\text{trans}} = \rho_{\text{trans}} \frac{w}{A} = \frac{V_{\text{trans}}}{I_{\text{q}}}, \tag{2.8}$$

where $A = w \cdot l$ is the cross-section of the sample, t the thickness of the conducting layer, V_{trans} the voltage drop transverse to the current direction and I_{q} the current through the Hall bar.

For ferromagnetic conductors and paramagnetic conductors within a magnetic field, there is an additional contribution, depending directly on the magnetization M of the material. This contribution is called the anomalous Hall effect(AHE) and can be taken into account by modifying Eq. (2.7) to include a magnetization-dependent term which yields Eq. (2.9) [5]:

$$\rho_{\text{H}} = A_{\text{OHE}} B + A_{\text{AHE}} M(T, H) \tag{2.9}$$

The ordinary Hall coefficient A_{OHE} is the same as the one introduced in Eq. (2.7). The so called anomalous Hall coefficient A_{AHE} can be explained by the theory developed in 1954 by Karplus and Luttinger [3], and in a more recent approach, using the Berry-phase developed by Berry in 1984 [4].

2.5 Spin Hall AHE

Y. T. Chen proposed a Spin Hall AHE due to the imaginary part of the spin mixing interface conductance $G_{\uparrow\downarrow}$ [15] in ferromagnetic insulator (FMI)/normal metal (NM) hybrid structures. Starting from the spin diffusion equation one can derive an equation for the change of the transverse specific resistance $\Delta\rho_2$

$$-\Delta\rho_2 \approx 2\Theta_{\text{SH}}^2 \frac{\lambda^2}{t_{\text{NM}}} \frac{G_{\text{i}} \tanh^2 \frac{\lambda}{2t_{\text{NM}}}}{\left(\sigma + 2G_{\text{r}}\lambda \cosh \frac{\lambda}{t_{\text{NM}}}\right)^2}, \tag{2.10}$$

where Θ_{SH} is the spin-Hall angle, λ the spin diffusion length, t_{NM} is the thickness of the normal metal film and $\sigma = \frac{1}{\rho_0}$ the "intrinsic electric resistivity of the bulk normal metal" [15], $G_{\text{r}} = \text{Re}(G_{\uparrow\downarrow})$ the real part and $G_{\text{i}} = \text{Im}(G_{\uparrow\downarrow})$ the imagninary part of the spin mixing interface conductance $G_{\uparrow\downarrow}$ [15,24].

The parameters for hybrid structures with YIG as FMI and platinum as NM (c.f. inset in Fig. 2.6 and Sec. 3.1) were measured by Althammer *et al.* [13]. Using these parameters, one can plot the curve of the expected change of the transverse specific resistance $\Delta\rho_2$ due to the spin Hall anomalous Hall effect at 300 K. This is shown in Fig. 2.6. The curve peaks at $t_{\mathrm{Pt}} = 2\lambda$ and decays for $t_{\mathrm{Pt}} \to \infty$.

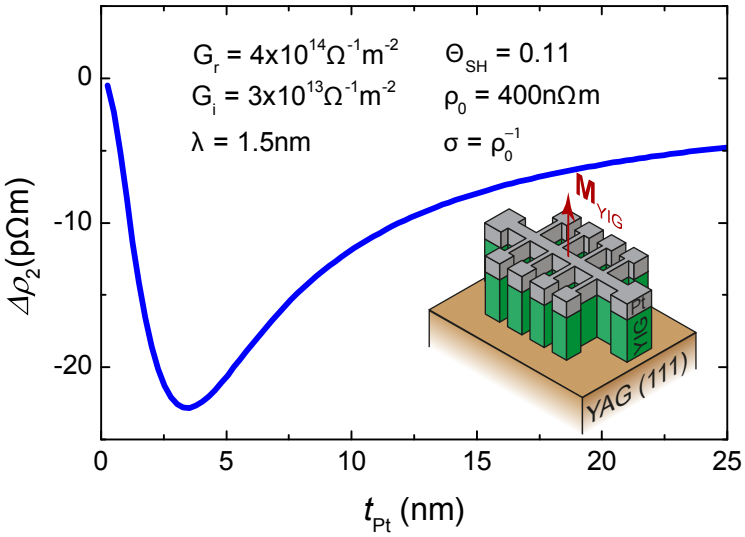

Figure 2.6: Theory curve for the spin Hall anomalous Hall effect as predicted by Chen *et al.* [15] using the parameters quoted by Althammer *et al.* [13].

Chapter 3

Experimental Methods and Setup

In this chapter, the sample preparation (Sec. 3.1) and the magnet setups (Sec. 3.2) will be shown. Furthermore, the experimental methods applied during the measurements are described in Sec. 3.3.

3.1 Sample Preparation

The YIG/Pt hybrid structures were grown on (111)-oriented gadolinium gallium garnet (GGG[1]) or yttrium aluminum garnet (YAG[2]) substrates.[3] The epitaxial YIG films with thicknesses of $50-60\,\mathrm{nm}$ were deposited using pulsed laser deposition [26]. The polycrystalline platinum films ($1-20\,\mathrm{nm}$) evaporated on the YIG films in-situ (without breaking the vacuum) using electron beam evaporation. The layered structure of the samples after growth is shown in Fig. 3.1.

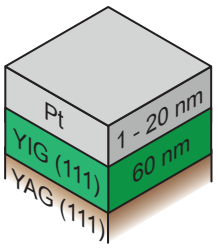

Figure 3.1: Structure of the used YIG/Pt samples.

After cutting the samples in halves, a Hall bar structure, as shown in Fig. 3.2, was patterned into the samples utilizing photolitography[4] and subsequent argon ion beam milling. The width of the Hall bar is $w = 80\,\mu\mathrm{m}$ and the total length is $1000\,\mu\mathrm{m}$. The

[1] $Gd_3Ga_5O_{12}$
[2] $Y_3Al_5O_{15}$
[3] The hybrid structures were grown by Sibylle Meyer and Marc Schneider
[4] The photoresist used to coat the samples was AZ 5214E, that was annealed for 70 s at 110 °C. The resist was then exposed to UV light (by a mercury vapour lamp) for 40 s and developed in pure AZ 726 MIF developer for 60 s.

distance between two contacts along the long direction is 200 µm, so the total length between the longitudinal voltage V_{long} sensing contacts (c.f. Fig. 3.2 and Fig. 3.6) is $l = 600\,\mu\text{m}$.

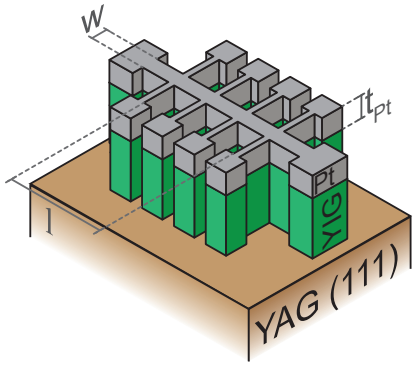

Figure 3.2: Structure of the samples after patterning. For the used samples, the length is $l = 600\,\mu\text{m}$, the width is $w = 80\,\mu\text{m}$ and the thickness ranges between $t_{\text{Pt}} = 0.8\,\text{nm}$ and $t_{\text{Pt}} = 21.5\,\text{nm}$. In analogy to [13]

After patterning, the samples were glued to a chip carrier with GE Varnish directly on top of a copper cuboid acting as heatsink and bonded with aluminum wires. A mounted and bonded sample is shown in Fig. 3.3, the copper cuboid is visible inbetween the connector pins. All samples used during this thesis are shown in Tab. B.1.

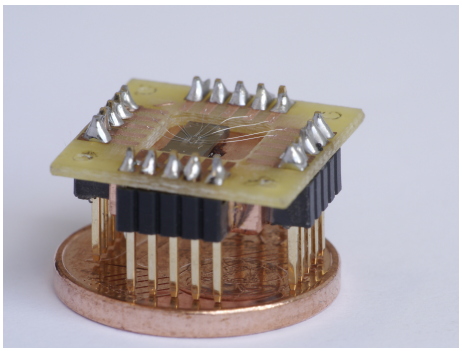

Figure 3.3: Sample on chip carrier after being glued to the copper cuboid with GE Varnish and bonded with aluminum wires. Figure provided by D. Irber (Ref [14]).

3.2 Magnet Setup

3.2.1 Room Temperature Electromagnet

The first measurements of the ordinary Hall coefficient were conducted in a room temperature electromagnet setup. The magnet is controlled by a LakeShore Gauss meter, with a Hall probe mounted directly at one pole shoe for feedback regulation, reaching an accuracy of $\Delta(\mu_0 H) < 0.1\,\text{mT}$.

The two copper coils of the magnet allow fields of up to $\mu_0 H = 1.2\,\mathrm{T}$, though, for safety reasons and to keep the variation of the room temperature to a minimum, only fields up to $\mu_0 H = 0.5\,\mathrm{T}$ were used during this thesis.

To allow for the rotation of the electromagnet around the sample, the chip carriers were mounted on top of a dipstick. The mounting geometry is depicted in Fig. 3.4. Additionally, the LakeShore Gauss meter measures the temperature in close proximity to the dipstick, providing insight into temperature stability of the room.

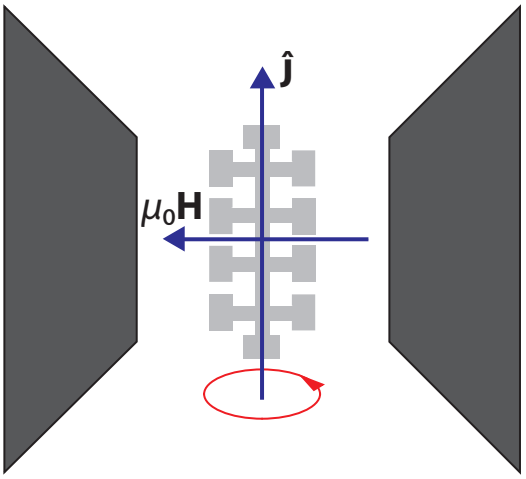

Figure 3.4: Mounting of the samples in out of plane geometry (oopj) between the pole shoes of the magnet (gray surfaces).

3.2.2 Magnet Cryostat

The rotation and extended field sweep measurements were carried out in an Oxford Instruments SM4000-8 magnet cryostat. The maximal magnetic field of $\mu_0 H = 7\,\mathrm{T}$ is generated by a pair of superconducting split-coils. The temperature within the variable temperature insert (VTI), where the sample is mounted on a dipstick, can be set from $T_{\mathrm{VTI}} = 1.5\,\mathrm{K}$ to $T_{\mathrm{VTI}} = 300\,\mathrm{K}$.

The VTI is evacuated by a membrane pump, a needle valve regulates the flow of helium and a resistive heater controls the temperature inside the insert.

The chip carriers are mounted on a dipstick with a seperate temperature control by a LakeShore temperature controller. The chip carriers are thermally coupled to the dipstick via heat conducting paste, so one can assume the same temperature for the sample as for the dipstick.

The dipstick can be rotated by 360° with an Owis DMT 100 stepper motor. Furthermore it allows mounting of the samples in three different geometries (field in plane, field out of plane rotating around **t** and field out of plane rotating around **j**, c.f. Fig. 3.5), though only the out of plane orientation (oopj) shown in Fig. 3.5 was used during this thesis.

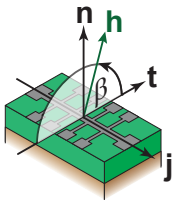

Figure 3.5: Definition of the coordinate system for out of plane rotations around **j**. In analogy to [13].

The controls of the LakeShore temperature controller, the cryostat's temperature controller (Oxford Instruments Intelligent Temperature Control, ITC), the magnetic field (via an Oxford Instruments Intelligent Power Supply, IPS) and the stepper motor were performed with Labview-based software. For further information see [27].

3.3 Measurement Techniques

The current I_q along the Hall bar is driven by a Keithley K2400 SourceMeter. The transverse and longitudinal voltages are measured by two Keithley K2182 Nanovoltmeters (c.f. Fig. 3.6). The setup allows for the application of the delta method, where the voltage is measured twice, once for a positive current and once for a negative current. The voltage is then calculated by [28]

$$V_{\text{delta}} = \frac{V(I_q) - V(-I_q)}{2}. \tag{3.1}$$

Therefore, the original sign of the voltage for a positive current is retained even after the calculation. The delta method is used to reduce systematic errors, as all contributions that are independent of (or symmetric in) I, e.g. thermal voltages, are cancelled out.

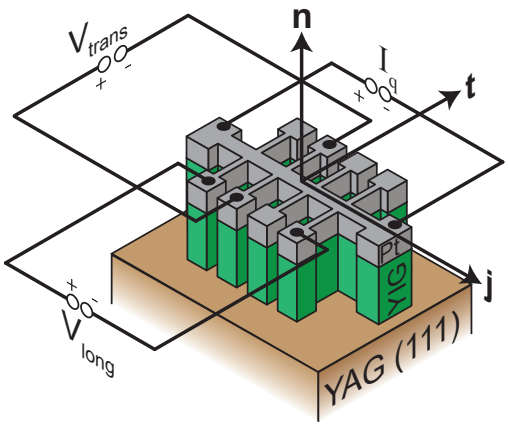

Figure 3.6: Connection diagram of the Hall bar including the used sign convention. In analogy to [13]

Chapter 4

Results and Discussion

The measurements performed during this thesis focussed on evaluating the Hall effect in YIG/Pt hybrid structures. The transverse voltage V_{trans} across the Hall bar structure (c.f. Fig. 3.6) was measured, while applying a magnetic field $\mathbf{H}$ perpendicular to the film plane. This so called "Hall voltage" contains two contributions, one from the ordinary and one from the extraordinary(anomalous) Hall effect.

Although no anomalous Hall effect is expected in (paramagnetic) platinum, we observed an anomalous Hall-like effect, and attribute it to the spin Hall AHE (c.f. Sec. 2.5). We therefore referenced the corresponding coefficient to the magnetization $\mathbf{M}$ of the YIG film.

To distinguish between the ordinary Hall effect ($V_{\text{trans}} \sim \mu_0 \mathbf{H}$) and the anomalous Hall-like effect ($V_{\text{trans}} \sim \mathbf{M}$), we here use the term "anomalous Hall effect" for the signature caused by the presence of a ferromagnetic insulator attached to the normal metal. As the measurement geometry and the method for acquiring the anomalous Hall-like effect's contribution are similar, this analogy was chosen to make the topic more accessible. The focus will be on the platinum thickness dependence of both coefficients A_{OHE} and A_{AHE}.

Additionally, the anomalous Hall coefficient is explored in the context of the spin Hall magnetoresistance theory framework. This framework quantitatively explains the experiments concerning the longitudinal component of the magnetoresistance effect observed in YIG/Pt hybrid structures [12, 13, 29].

Different experimental approaches to estimate both coefficients were used. The discussion of the results will be split into three parts. First some assumptions made for the stray field of the YIG thin film shall be analyzed in Sec. 4.1. Then the ordinary Hall coefficient will be discussed in Sec. 4.3. This chapter will conclude with the investigation of the (spin Hall) anomalous Hall coefficient in Sec. 4.4.

4.1 Magnetization in Thin Ferromagnetic Films

One can assume that, in close proximity to the YIG film, a stray field is created by the magnetization of the ferromagnet. This resulting field at the YIG/Pt interface

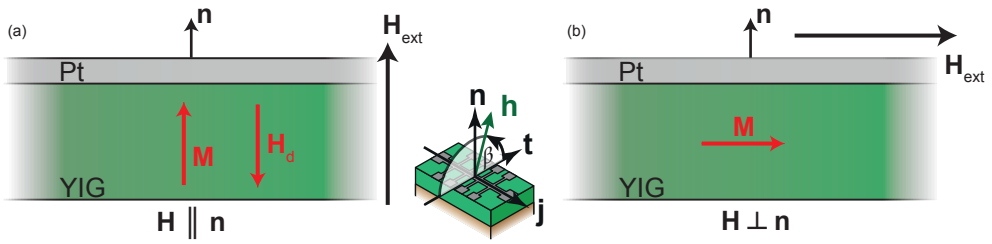

Figure 4.1: Effective field within an infinite sheet of a ferromagnetic material.
(a) With the external field pointing out of plane ($\mathbf{H}_{\text{ext}} \parallel \mathbf{n}$), the demagnetiaton field $\mathbf{H}_{\text{d}}$ is compensating the whole magnetization $\mathbf{M}$. Thus the magnetic field $\mathbf{B}$ inside the ferromagnetic material is $\mathbf{B} = \mu_0 \mathbf{H}_{\text{ext}}$. (b) With the external field pointing in plane ($\mathbf{H}_{\text{ext}} \perp \mathbf{n}$), no demagnetization field is created, as all magnetic flux lines are within the ferromagnetic material. Here, the internal magnetic field is $\mathbf{B} = \mu_0(\mathbf{H}_{\text{ext}} + \mathbf{M})$.

shall be discussed, as it could be one possible reason for the observed anomalous Hall effect (Sec. 4.4) in the platinum film.

If a ferromagnetic material has a magnetization, a surface charge is generated on its faces perpendicular to $\mathbf{M}$. The potential due to this charge creates the demagnetization field $\mathbf{H}_{\text{d}}$. The magnetic field $\mathbf{B}$ within a saturated ferromagnetic material in an external field $\mathbf{H}_{\text{ext}}$ (uniform magnetization $\mathbf{M}_{\text{sat}} \parallel \mathbf{H}_{\text{ext}}$), taking into account the demagnetization field is [25]

$$\mathbf{B}_{\text{i}} = \mu_0(\mathbf{H} + \mathbf{M}_{\text{sat}}) = \mu_0(\mathbf{H}_{\text{ext}} + \mathbf{M}_{\text{sat}} + \mathbf{H}_{\text{d}}). \tag{4.1}$$

The demagnetization field of an arbitrary shaped body can be described by the demagnetization tensor $\hat{\mathbf{N}}$ and the magnetization $\mathbf{M}_{\text{sat}}$ [30]:

$$\mathbf{H}_{\text{d}} = -\hat{\mathbf{N}}\mathbf{M}_{\text{sat}} = -\begin{pmatrix} N_{\text{jj}} & N_{\text{jt}} & N_{\text{jn}} \\ N_{\text{tj}} & N_{\text{tt}} & N_{\text{tn}} \\ N_{\text{nj}} & N_{\text{nt}} & N_{\text{nn}} \end{pmatrix} \mathbf{M}_{\text{sat}}. \tag{4.2}$$

The demagnetization field is linear in the magnetization with an opposite sign.

To estimate the field at the surface of the ferromagnetic insulator, at first, the simplest possible assumption of an infinite sheet was made. This simplification, reducing the problem to two dimensions ($\mathbf{j}$ and $\mathbf{t}$ are similar in this case), allows to make a rough estimate. For an infinite sheet only $N_{\text{nn}} = 1$ is non-vanishing [31].

Therefore, the magnetic field inside the ferromagnetic material B can be written as

$$\frac{(B_{\mathrm{int}})_{\mathrm{j}}}{\mu_0} = (\mathbf{H}_{\mathrm{ext}})_{\mathrm{j}} + (\mathbf{M}_{\mathrm{sat}})_{\mathrm{j}} - N_{\mathrm{jj}}(\mathbf{M}_{\mathrm{sat}})_{\mathrm{j}} \overset{\text{inf. sheet}}{=\!=} (\mathbf{H}_{\mathrm{ext}})_{\mathrm{j}} + (\mathbf{M}_{\mathrm{sat}})_{\mathrm{j}}, \tag{4.3}$$

$$\frac{(B_{\mathrm{int}})_{\mathrm{t}}}{\mu_0} = (\mathbf{H}_{\mathrm{ext}})_{\mathrm{t}} + (\mathbf{M}_{\mathrm{sat}})_{\mathrm{t}} - N_{\mathrm{tt}}(\mathbf{M}_{\mathrm{sat}})_{\mathrm{t}} \overset{\text{inf. sheet}}{=\!=} (\mathbf{H}_{\mathrm{ext}})_{\mathrm{t}} + (\mathbf{M}_{\mathrm{sat}})_{\mathrm{t}}, \tag{4.4}$$

$$\frac{(B_{\mathrm{int}})_{\mathrm{n}}}{\mu_0} = (\mathbf{H}_{\mathrm{ext}})_{\mathrm{n}} + (\mathbf{M}_{\mathrm{sat}})_{\mathrm{n}} - N_{\mathrm{nn}}(\mathbf{M}_{\mathrm{sat}})_{\mathrm{n}} \overset{\text{inf. sheet}}{=\!=} (\mathbf{H}_{\mathrm{ext}})_{\mathrm{n}}\,, \tag{4.5}$$

where $(\mathbf{M}_{\mathrm{sat}})_{\mathrm{j}}$ denotes the $\mathbf{j}$ component of the vector $\mathbf{M}_{\mathrm{sat}}$, i.e., $(\mathbf{M}_{\mathrm{sat}})_{\mathrm{j}} = \mathbf{M}_{\mathrm{sat}} \cdot \mathbf{j}$.

Knowing the internal magnetic field, one can use the boundary conditions for the **B**- and the **H**-field [32]:

$$(\mathbf{B}_{\mathrm{ext}} - \mathbf{B}_{\mathrm{int}}) \cdot \mathbf{n} = 0, \tag{4.6}$$

$$(\mathbf{H}_{\mathrm{ext}} - \mathbf{H}_{\mathrm{int}}) \times \mathbf{n} = 0. \tag{4.7}$$

Therefore, for the external field pointing out of plane ($\mathbf{H}_{\mathrm{ext}} \parallel \mathbf{n}$), the boundary condition for the **B**-field is fulfilled, and the internal field $\mathbf{B}_{\mathrm{int}}$ equals the external field $\mathbf{B}_{\mathrm{ext}} = \mu_0 \mathbf{H}_{\mathrm{ext}}$. This situation is shown in Fig. 4.1(a). For the external field pointing in plane ($\mathbf{H}_{\mathrm{ext}} \perp \mathbf{n}$), the boundary condition for **H** is fulfilled. The internal field $\mathbf{H}_{\mathrm{int}}$ equals the external field $\mathbf{H}_{\mathrm{ext}}$. This case is displayed in Fig. 4.1(b). The respective other boundary condition is neglected, as it is never reached by the fields (the boundary is at infinity).

So, resulting from the simplification of the Hall bar as an infinite sheet, the magnetic stray field of the ferromagnetic material's magnetization is totally compensated. Since this was only a rough estimation of the real situation, the significance of the result might still appear questionable.

Thus, another attempt to calculate a more accurate behaviour was made. Aharoni [31] derived equations for the demagnetization tensor of a rectangular prism. The demagnetization tensor is in this case diagonal with three non-vanishing components N_{jj}, N_{tt} and N_{nn}. These equations, however, can only be applied at the center of the coordinate system ($j = t = 0$ for $\mathbf{H}_{\mathrm{ext}} \parallel \mathbf{n}$), thus still being only estimates for the real situation in the Hall bar. From these equations, the demagnetization factors close to the surface [1] of the rectangular prism were calculated to be $N_{\mathrm{jj}} = 0.00179456$, $N_{\mathrm{tt}} = 0.0238858$ and $N_{\mathrm{nn}} = 0.997861$ for Hall bar dimensions of $l_{\mathrm{j}} = 1000\,\mu\mathrm{m}$ (long side), $w_{\mathrm{t}} = 80\,\mu\mathrm{m}$ (short side) and $t_{\mathrm{n,YIG}} = 60\,\mathrm{nm}$ (thickness).

Finally, with the refined version of the demagnetization tensor, one can see, that the assumption of the infinite film was not bad after all. These values allow to use

[1] $z/c = 0.99$, where z is the height in $\mathbf{H}_{\mathrm{ext}}$ direction from the center of the Hall bar, and c half the length of the rectangular side parallel to $\mathbf{H}_{\mathrm{ext}}$

equations Eq. (4.3) to Eq. (4.5) to obtain the field for an arbitrary external field (as long as it is big enough to saturate M_{YIG}).

Now, our experimental conditions and the possible impact of the preceeding discussion shall be investigated. With an external field of $\mu_0 H_{\mathrm{ext}} = 1\,\mathrm{T}$[2], the YIG film is fully saturated ($\mu_0 H_{\mathrm{sat,YIG}} \approx 200\,\mathrm{mT}$ [33]). Furthermore a field of this magnitude is ensuring, that the YIG's magnetization aligns parallel with the external field ($\mathbf{H} \parallel \mathbf{M}_{\mathrm{YIG}}$).

The saturation magnetization of all YIG films used during this thesis is assumed to be $M_{\mathrm{sat}} = 120\,\mathrm{kA\,m^{-1}}$ [26]. Using these values, Eq. (4.3) to Eq. (4.5) and the demagnetization coefficients, one can calculate, that in out of plane geometry ($\mathbf{H}_{\mathrm{ext}} \parallel \mathbf{n}$) the field at the YIG/Pt interface is

$$B = \mu_0(H_{\mathrm{ext}} + M_s - 0.997861 M_s) = \mu_0 H_{\mathrm{ext}} + 0.32\,\mathrm{mT} \tag{4.8}$$

As $\Delta B = 0.32\,\mathrm{mT} << \mu_0 H_{\mathrm{ext}}$, it is neglected in all further evaluations.

Furthermore, it is assumed, that the magnetization of platinum due to paramagnetic ordering ($\chi_{\mathrm{v,Pt}} = 19.3 \times 10^{-6}$ [32]) is much smaller than the external field ($M_{\mathrm{Pt}} << H_{\mathrm{ext}}$). Thus, resulting from this preliminary discussion, the field relevant to the ordinary Hall effect is $\mu_0 H_{\mathrm{ext}}$.

4.2 Thickness dependece of ρ_0

To compare the experimental data to the predictions made by the SMR theory framework, one needs to include the thickness dependence of the resistivity in Eq. (2.10). Fischer *et al.* [34] extended the Fuchs-Sondheimer Theory [35] and derived, that the thickness dependence of the sheet resistance of a thin platinum film can be written as

$$\rho_0(t_{\mathrm{Pt}}) = \rho_\infty \left(1 + \frac{3 l_\infty}{8(t_{\mathrm{Pt}} - h)}(1 - p)\right) \tag{4.9}$$

for $t_{\mathrm{Pt}} > h$, where h is the mean surface roughness of the platinum film, ρ_∞ the bulk resistivity for platinum, and l_∞ the electron mean free path in bulk platinum. The parameter p represents scattering at the interfaces, which is neglected here ($p = 0$), as it was also done by Althammer *et al.* [13].

Figure 4.2 shows the data recorded for ρ_0 during rotations of the YIG/Pt hybrid structures in a fixed magnetic field. Equation (4.9) was fitted to the data (black line), and the resulting parameters are denoted in the figure. As the trend of the data is

[2] A magnetic field of $\mu_0 H_{\mathrm{ext}} = 1\,\mathrm{T}$ was used during the angle dependent measurements of the transverse voltage V_{trans}, where the YIG/Pt hybrid structures were rotated in a fixed magnetic field, c.f. Sec. 4.4.

reproduced by the fit, the assumption of no interface scattering ($p = 0$) seems to be valid. Thus, it is now possible to include Eq. (4.9) with the gathered parameters into Eq. (2.10). This was done for the theory curve shown in Fig. 4.12.

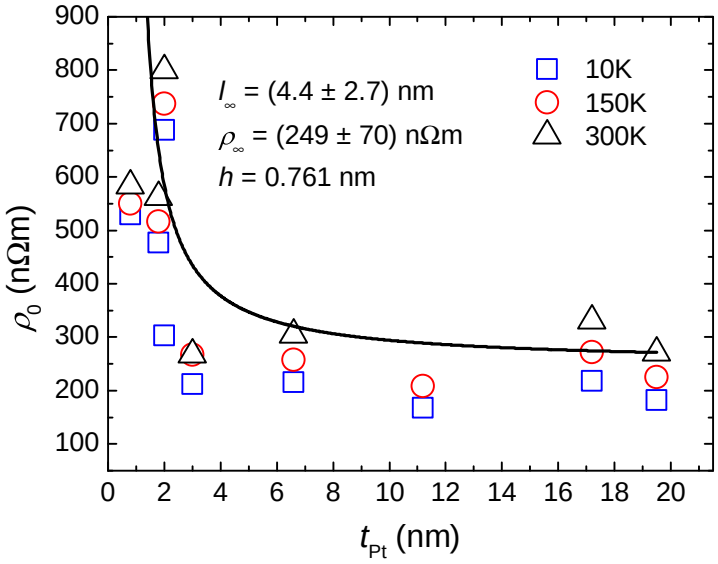

Figure 4.2: Thickness dependence of the measured longitudinal sheet resistances of YIG/Pt hybrid structures. The black line is a fit of Eq. (4.9) to the data,using the parameters denoted in the graph.

4.3 Ordinary Hall Coefficient

In Fig. 4.3(a) an angle dependent measurement of both, the longitudinal voltage V_{long} and the transverse voltage V_{trans}, when rotating the magnetic field out of plane perpendicular to $\mathbf{j}$ (oopj, c.f. insert in Fig. 4.3). The $\cos^2(\beta)$ dependence in the longitudinal signal (black squares) due to the longitudinal spin Hall magnetoresistance (SMR, c.f. Sec. 2.3) effect is clearly visible, whereas the transverse signal (blue triangle) follows a $\sin\beta$, exhibiting the expected behaviour for Hall type measurements (c.f. Eq. (2.6)). Now, the position of the Hall bar with respect to the magnetic field was chosen, that both, the longitudinal as well as the transverse signal, have a maximum (indicated by the red line in Fig. 4.3(a)). This corresponds to the Hall geometry (c.f. Fig. 2.5), where the external field vector $\mathbf{H}$ points (anti)parallel to the normal vector of the sample plane ($\mathbf{n} \parallel \mathbf{H}$). Resulting from this assumption, a maximal Hall signal is expected.

As the sample alignment plays a crucial role for Hall type measurements, since slight tilts out of the out of plane configuration ($\mathbf{H} \parallel \mathbf{n}$) cause non-vanishing in plane

projections of the magnetization and thus give rise to other type of effects[3]. Therefore, the procedure described above is necessary, since the chip carrier is mounted on top of a dipstick and therefore the sample plane can not be seen by the eye.

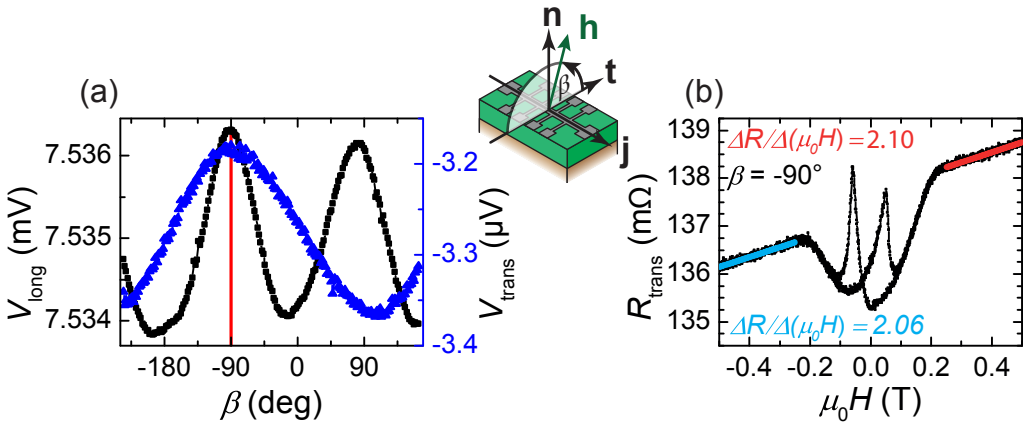

Figure 4.3: (a) Orientation of the sample using the longitudinal spin Hall magnetoresistance (SMR) effect in oopj rotation geometry (see insert). According to SMR theory, the magnetic field orientation, where both, the longitudinal and the transverse voltage, have a maximum. This is, where **H** is pointing in $-\mathbf{n}$ direction. The applied field was $\mu_0 H = 1000\,\mathrm{mT}$. (b) Measurement of the transverse resistivity during a field sweep from $\mu_0 H = -0.5\,\mathrm{T}$ to $\mu_0 H = 0.5\,\mathrm{T}$ and back. The broad dips are caused by transverse magnetoresistance, also observed by [12], when the magnetization of the YIG film is rotating through the film. The narrower peaks are due to the rotation of the magnetization within the plane. The cyan and red lines represent linear fits in the positive and negative saturation regime from which the ordinary Hall coefficient is determined.

Having aligned the Hall bar with respect to the magnetic field, the transverse voltage was measured during a field sweep ranging from $\mu_0 H = -500\,\mathrm{mT}$ to $\mu_0 H = 500\,\mathrm{mT}$ in 1 mT steps. The maximum magnetic field $\mu_0 H = 500\,\mathrm{mT}$ was chosen, as the YIG's magnetization is saturated at $\mu_0 H_{\mathrm{sat,YIG}} \approx 200\,\mathrm{mT}$ [33], allowing to reliably determine the slope in both saturation regimes.

The resistance R_{trans} was calculated via division of the measured voltages by the driving current. The current was fixed to $I = 100\,\mu\mathrm{A}$, to ensure that joule heating of the Hall bar is negligibly small. The broad dip from $\mu_0 H = -200\,\mathrm{mT}$ to $\mu_0 H = 200\,\mathrm{mT}$ within Fig. 4.3(b) is due to transverse magnetoresistance, when the YIG's magnetization has a non-vanishing component in plane, whereas the narrower peaks results from the rotation of the magnetization within the YIG film plane. This

[3]For example, if $m_j \neq 0$, a $\sin^2(\beta)$ dependent sign is superimposed on the transversal voltage following Eq. (2.6).

was also measured by Nakayama *et al.* and is shown in their paper [12] in fig. 4(b). The slope $\frac{\mathrm{d}}{\mathrm{d}B}R_{\mathrm{trans}}$ was then calculated via linear fits in the positive as well as the negative saturation regime, indicated in Fig. 4.3(b).

Then, one can calculate the ordinary Hall coefficient using Eq. (2.8) including the measured slope

$$A_{\mathrm{OHE}} = \frac{\mathrm{d}R_{\mathrm{trans}}}{\mathrm{d}B} t_{\mathrm{Pt}}. \tag{4.10}$$

In the saturation regime, the anomalous Hall effect, assumed to scale with $\mathbf{M}$, should be constant, such that the slope in the saturation regime only reflects the ordinary Hall effect. The same procedure was performed for several YIG/Pt hybrid structures with platinum thicknesses between $t_{\mathrm{Pt}} = 2\,\mathrm{nm}$ and $t_{\mathrm{Pt}} = 19.5\,\mathrm{nm}$.

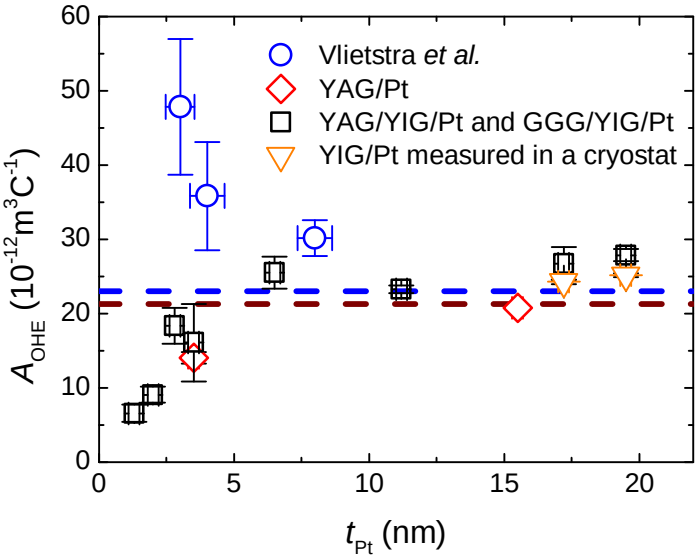

Figure 4.4: Measured ordinary Hall coefficient A_{OHE} plotted against the thickness of the platinum film. YIG/Pt hybrid structures in black, platinum on YAG in red, data measured by Vlietstra *et al.* [36] in blue. The orange triangles are values of the ordinary Hall coefficient measured within the cryostat. The two dashed lines represent two literature values for the Hall coefficient for bulk platinum at room temperature [37] [38]. The sample with $t_{\mathrm{Pt}} = 0.8\,\mathrm{nm}$, showing a sign change at room temperature (c.f. Fig. 4.7) was not analyzed in this setup, as it was grown after the experiments were finished.

The resulting ordinary Hall coefficients are plotted against the thickness of the platinum film in Fig. 4.4 as black squares. The errors were estimated by calculating the mean value of the slopes in the positive and the negative saturation regime and applying a student-T distribution to obtain the corrected standard deviation of the mean value.

The thickness of the platinum films was determined by high resolution x-ray diffraction (HRXRD) [26]. Therefore, an error for the platinum thicknesses of $\Delta t_{\mathrm{Pt}} = 0.2\,\mathrm{nm}$ is assumed. These errors are applied as error bars in Fig. 4.4. The orange triangles represent values measured using the magnet cryostat (c.f. Sec. 4.4). The two dashed lines correspond to two literature values for the ordinary Hall coefficient of bulk platinum measured by C. M. Hurd (blue, [38]) and D. Greig and D. Livesey (dark red, [37]). The measured ordinary Hall coefficient in Fig. 4.4 corresponds well to the literature for thick platinum films, whereas an additional contribution to A_{OHE} is found for very thin platinum films. This is unexpected as the ordinary Hall coefficient $A_{\mathrm{OHE}} = \frac{1}{ne}$ is not depending on the thickness of the platinum layer. One possible explanation are finite size effects on the band structure of the platinum layer. This is backed, as our reference sample without a ferromagnetic insulator layer (i.e. a 3.5 nm thick platinum layer directly evaporated on YAG) also shows a deviation from the literature value (red diamond).

We now compare our measurements to a recent publication by Vlietstra *et al.* [36]. Their data is shown in Fig. 4.4 in blue symbols. Vlietstra *et al.* also measured a deviation from the constant Hall coefficient A_{OHE} for thin platinum films, but with a different trend: as increase of A_{OHE} with $\frac{1}{t_{\mathrm{Pt}}}$. One might argue that Vlietstra *et al.* saw a different effect, since the used platinum was sputtered, and not evaporated like the platinum used during this thesis. Additionally, after growing the YIG films, the vacuum was broken and thus the FMI/NM interface might be contaminated with unwanted elements, changing the interface parameters. It should also be noted, that the platinum used by Vlietstra *et al.* displays a much higher ordinary Hall coefficient for thick samples ($A_{\mathrm{OHE}} \approx 30\,\mathrm{m^3\,C^{-1}}$ for $t_{\mathrm{Pt}} = 35\,\mathrm{nm}$), when compared to the literature, which indicates a lower free charge carrier density and thus a worse quality of the platinum.

Figure 4.5 shows another approach to the measurement of the t_{Pt}-dependence of A_{OHE}. It shows the "theoretical Hall thickness"

$$t_{\mathrm{Hall}} = \frac{0.23 \times 10^{-10}\,\mathrm{m^3\,C^{-1}}}{A_{\mathrm{OHE}}} t_{\mathrm{Pt}}. \tag{4.11}$$

plotted against the thickness obtained by HRXRD reflectometry. t_{Hall} represents the thickness of a sample, calculated using the literature value provided by C. M. Hurd [38] for bulk platinum as ordinary Hall coefficient. For platinum thicknesses $t_{\mathrm{Pt}} > 3\,\mathrm{nm}$ the calculated points are close to the red line, indicating no additional term, as the Hall thickness t_{Hall} equals the thickness obtained by reflectometry of the samples. For thicknesses $t_{\mathrm{Pt}} < 3\,\mathrm{nm}$ the Hall thickness assumes a constant value of $t_{\mathrm{Hall}} \approx 5\,\mathrm{nm}$, indicating additional contributions to the Hall coefficient. The two values for larger thicknesses ($t_{\mathrm{Pt}} > 15\,\mathrm{nm}$) deviate stronger from the red line in the

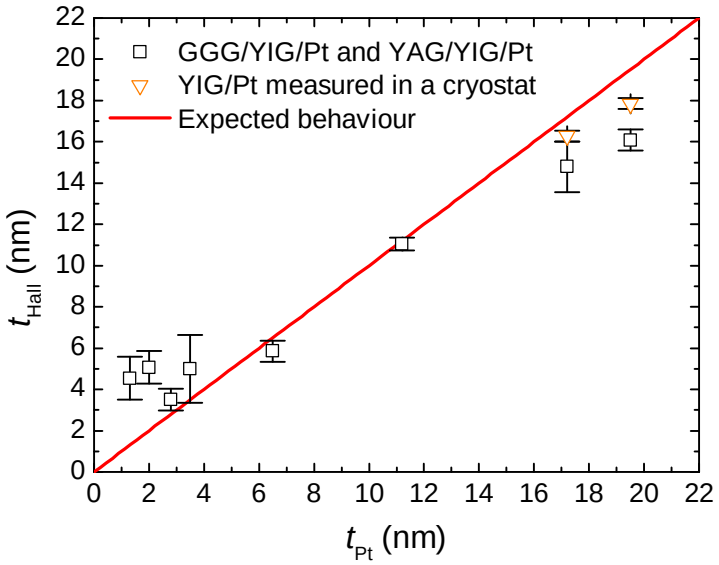

Figure 4.5: Calculated "Hall thickness" plotted vs the physical thickness obtained by high resolution x-ray diffraction. The Hall thickness was obtained by assuming the literature value [38] for the Hall coefficient and then calculating the samples' theoretical thickness from Eq. (4.11). The red line represents the expected behaviour, assuming there are no additional effects. The errors of the measured thickness t_{Pt} correspond to the symbol size of the shown data. The blue data were measured in the cryostat at $T = 300\,\mathrm{K}$ to probe the influence of thermal effects in the room temperature setup.

room temperature setup (black squares), than in the cryostat (orange triangles). Therefore, it is shown that there also is an error due to thermal drift in the room temperature setup, as the same samples were used for both measurements.

Through this plot, one can exclude systematic errors of the electron beam evaporation process, as the values for greater thicknesses correspond very well to the Hall thickness, thus indicating a good determination of the thickness by reflectometry. Additionally, it is highly unlikely, that, for all samples with a thickness of less than 3 nm, the systematic error increases with decreasing film thickness. Furthermore, dead platinum layers (insulating layers) would result in a deviation of the curve in the opposite direction than the deviation that takes place, thus these can not account for the deviation observed. The mechanism causing the change of the ordinary Hall coefficient is yet unknown and needs to be investigated more thoroughly.

To get a better understanding of $A_{\mathrm{OHE}}(t_{\mathrm{Pt}})$, field sweeps were carried out in a magnet cryostat, to reduce thermal drift and reach higher magnetic fields. This was necessary, as the room temperature setup only had a thermal stability of $\sim 0.2\,\mathrm{K}$.

Platinum is very sensitive to temperature changes, which can be seen in its wide spread application as a temperature sensor. Thus, thermal drift was a major problem

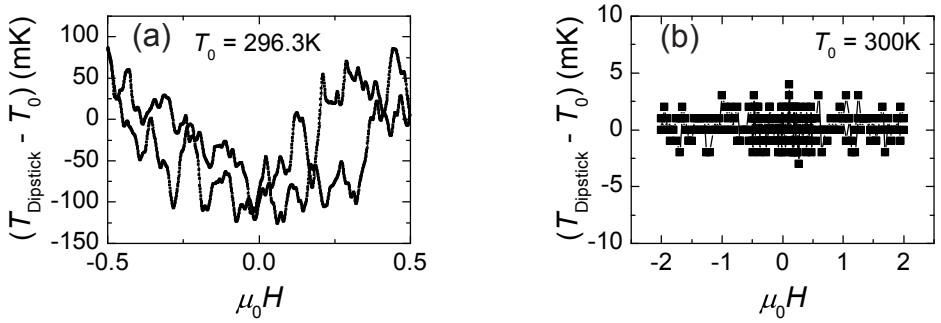

Figure 4.6: Temperature of the dipstick during a field sweep (a) in the room temperature setup and (b) in the cryostat setup.

during the measurements as shown in Fig. 4.6(a).
The temperature dependence of the resistivity can be described by

$$R(T) = R_0(1 + \alpha T). \tag{4.12}$$

R_0 is the resistance at $T = 0\,^{\circ}\mathrm{C}$ and α the temperature coefficient of the resistivity. Using Eq. (4.12) with $\alpha_{\mathrm{Pt}} = 3.92 \times 10^{-3}\,\mathrm{K}^{-1}$ [39] one obtains, that the resistivity of the platinum film changes by $\frac{\Delta R}{R_0} \approx 7.84 \times 10^{-4}$ for a temperature change of $\Delta T = 0.2\,\mathrm{K}$. The longitudinal SMR effect produces a $\frac{\Delta R_{\mathrm{SMR}}}{R_0} \approx 2.7 \times 10^{-4}$ for the sample shown in Fig. 4.3(a). If the temperature changes rapidly, it is therefore hard to observe the wanted effect. The change of the longitudinal signal is partially added to the transverse signal due to crosstalk. This crosstalk is caused by slight misalignment of the sample with respect to the magnetic field and because there is a small displacement between the transverse voltage sensing pads in longitudinal direction.

Hence, to improve the measurement's significance, they were carried out in a cryostat in a second step. By stabilizing a fixed temperature for 30 min before each measurement, one minimizes thermal effects within the resistivity of platinum. The temperature stability within the cryostat after themalization is $\sim \pm 3\,\mathrm{mK}$, as Fig. 4.6(b) shows.

The range of the sweeps was set from $\mu_0 H = -5\,\mathrm{T}$ to $\mu_0 H = 5\,\mathrm{T}$, to obtain a higher accuracy of the fit in the saturation regime. The maximum field of $\mu_0 H = 5\,\mathrm{T}$ was chosen, as no further information is obtained when proceeding to higher field. This can be seen in Fig. 4.7, where all samples show a linear dependence on the magnetic field for $\mu_0 H \gtrsim 1\,\mathrm{T}$. Furthermore the temperature dependence of the ordinary Hall coefficient was investigated by measuring the field sweeps at three

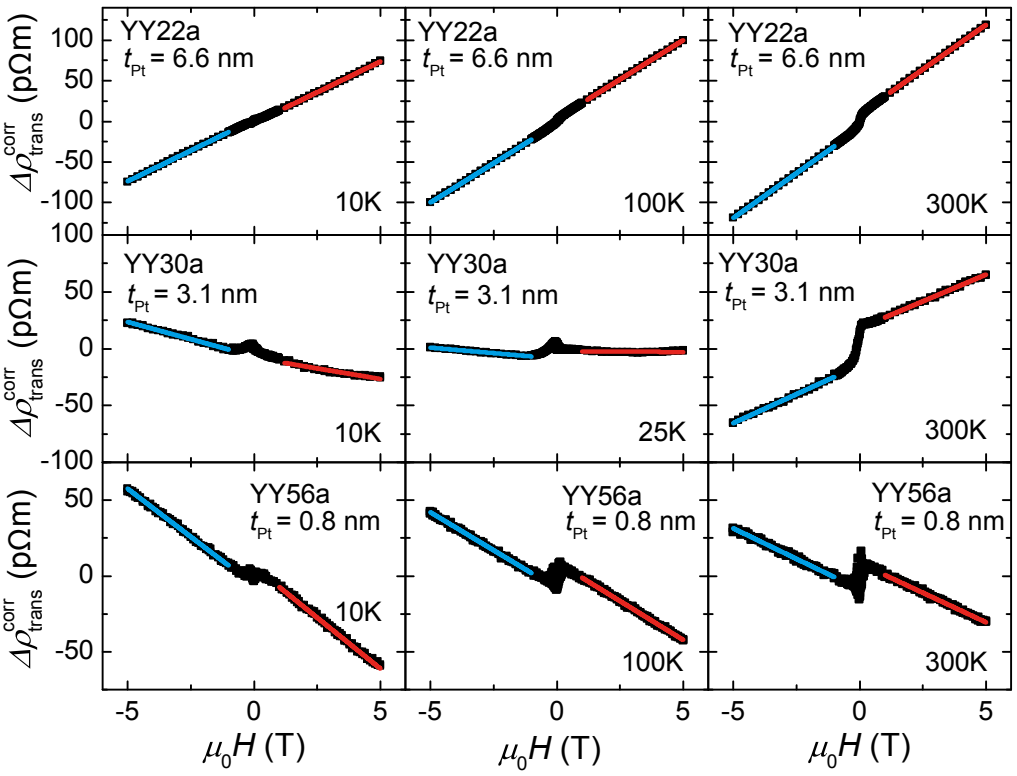

Figure 4.7: Measurement to determine the ordinary Hall coefficient A_{OHE} for three different temperatures and three different YIG/Pt hybrid structures. A sign change is observed when comparing the thicker platinum layer ($t_{\mathrm{Pt}} = 6.6\,\mathrm{nm}$, first row) to the thin platinum layer ($t_{\mathrm{Pt}} = 0.8\,\mathrm{nm}$, third row). If the thickness is chosen appropriately, this sign change within the ordinary Hall coefficient can be observed in one sample at different temperatures, as it is displayed in the second row. As the sample with $t_{\mathrm{Pt}} = 3.1\,\mathrm{nm}$ was not reconnected during the measurement procedure, artefacts as the origin of the sign change can be excluded.

different temperatures $T = 10, 100$ and $300\,\mathrm{K}$. The measurements were carried out the same way as in the room temperature setup:
After mounting the samples in out of plane geometry, they were oriented using the longitudinal SMR effect in an oopj rotation and the field sweeps were carried out.
For one sample ($t_{\mathrm{Pt}} = 3.1\,\mathrm{nm}$), a sign change of the ordinary Hall coefficient A_{OHE} from $300\,\mathrm{K}$ to $10\,\mathrm{K}$ was measured. This series is shown in Fig. 4.7(central row). One can see, that the sign change happens gradually with decreasing temperature. The switching temperature for this hybrid structure was around $T = 25\,\mathrm{K}$. The

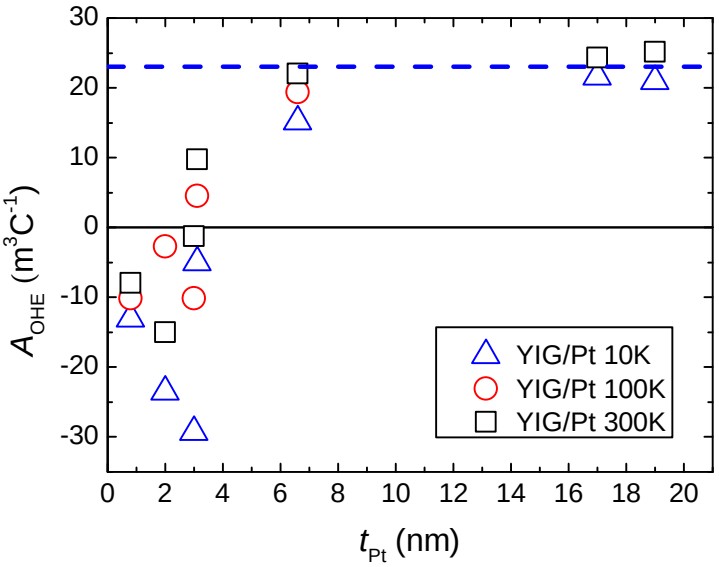

Figure 4.8: Measurement of the ordinary Hall coefficient plotted against the thickness t_{Pt} of the platinum film. The blue dashed line corresponds to the literature value for the Hall coefficient of bulk platinum [38].

corresponding measurement is shown in the central panel of Fig. 4.7.

The resulting ordinary Hall coefficients for all hybrid structures plotted against the thickness are shown in Fig. 4.8. The ordinary Hall coefficient is decreasing for lower platinum thicknesses, as it was also observed in the room temperature setup. Thus the change of the ordinary Hall coefficient is verified by the cryostat measurements performed at different temperatures. The magnitude of the change of the ordinary Hall coefficient, now determined more accurately, is larger than measured in the room temperature setup, leading to a sign change previously not observed. However, the sample with $t_{\mathrm{Pt}} = 2\,\mathrm{nm}$ is showing a high nonlinearity (c.f. Fig. B.1) in the saturation regime, making it hard to properly fit the slope in the saturation regime for 100 K and 300 K. This also explains the strange temperature behaviour, where the data point for 100 K is higher than the data point for 300 K, contrary to the behaviour of all other samples. The sign change shown in Fig. 4.7(central row) is also visible, when comparing very thin ($t_{\mathrm{Pt}} < 3\,\mathrm{nm}$) to thicker samples (at low temperatures). The switching temperature, at which the sign changes, is increasing with decreasing platinum thickness.

In Fig. 4.9 the measurements carried out in the magnet cryostat (black squares) are compared to the measurements taken with the room temperature setup (red hexagons). One can see, that the deviation is small for large thicknesses $t_{\mathrm{Pt}} > 6\,\mathrm{nm}$.

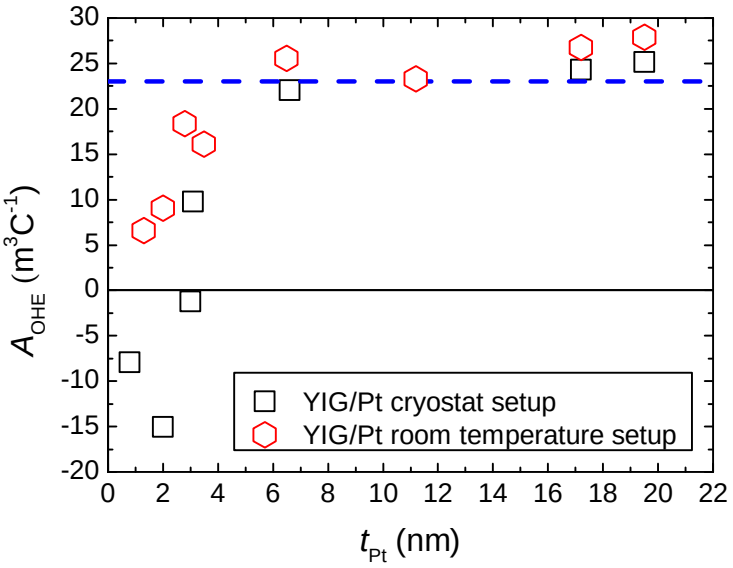

Figure 4.9: Comparative plot of the measurements in the magnet cryostat system and the room temperature electromagnet setup. The black squares represent data taken in the magnet cryostat, the red hexagons were measured in the room temperature setup. The dashed line corresponds to the literature value of the ordinary Hall coefficient for bulk platinum [38].

This deviation is most likely caused by thermal effects in the room temperature setup. However, for lower platinum thicknesses, the measurements do not agree very nicely, although the trend for decreasign signals with decreasing film thicknesses in both measurements is the same. The observed sign change at 300 K in the cryostat for the hybrid structures with $t_{\mathrm{Pt}} = 2\,\mathrm{nm}$ was not observed in the room temperature setup, whereas the samples with $t_{\mathrm{Pt}} = 0.8\,\mathrm{nm}$ and $t_{\mathrm{Pt}} = 3\,\mathrm{nm}$ were not analyzed in the room temperature electromagnet, as they were grown after the experiments were finished. The deviation of the sample with $t_{\mathrm{Pt}} = 2\,\mathrm{nm}$, as explained above, is due to the non linearity of the slopes in the saturation regime (c.f. Fig. B.1).

Thus, the better temperature stability of the magnet cryostat system supports the measurements made in the room temperature setup and verifies the additional term, although further investigations have to be done to probe the deviations of both measurements.

The observed change of the ordinary Hall coefficient is most likely caused by finite size effects, as the change was also observed in platinum layers without an underlying YIG film (c.f. red prisms in Fig. 4.4). When electron-surface scattering is the dominant scattering mechanism, the hall mobility μ_{H} is changed significantly, also

changing the ordinary Hall coefficient. This assumption is valid, as the mean free path of the electrons for bulk platinum is $L_\infty \approx 4\,\mathrm{nm}$ [13] and therefore larger than the thickness of the films. These finite size effects were also observed in thin gold films [40].

As platinum is a two band conductor [34], one can argue, that for very low thicknesses the electron conductivity collapses and the hole conductivity is dominant. This, however is contrary to the observations made by Fischer*et al.* [34], claiming, that the hole conductivity decrases much faster than the electron conductivity due to the hole's higher effective mass m_h^* and therefore larger scattering cross-sections.

We therefore suppose, that the band structure and thus the Fermi surface of the platinum changes significantly in films with very low platinum thicknesses $t_\mathrm{Pt} < 3\,\mathrm{nm}$.

4.4 Anomalous Hall Effect

We now turn to the anomalous Hall effect measured in YIG/Pt hybrid structures. To allow comparability, only the anomalous Hall effect's contribution to the specific resistance ρ_{AHE} is shown in this chapter instead of the anomalous Hall coefficient A_{AHE}, to simplify the comparison of the contributions of the ordinary and the anomalous Hall effect. One way to obtainρ_{AHE} is by making field sweeps. After fitting the slope in the saturation regime, one can interpolate back to $\mu_0 H = 0\,\mathrm{T}$ (this corresponds to the abscissa of the ordinary Hall fit curve). This procedure is depicted in Fig. 4.10. By doing this in both, the positive and negative saturation regime, one gets a $\Delta\rho_{\mathrm{trans}}(\mu_0 H = 0)$. To obtain the contribution of the anomalous Hall effect on the specific resistance, $\Delta\rho_{\mathrm{trans}}(\mu_0 H = 0)$ needs to be divided by 2:

$$\rho_{\mathrm{AHE}} = \frac{\Delta\rho_{\mathrm{trans}}(\mu_0 H = 0)}{2} \tag{4.13}$$

The Hall measurement of a reference sample with 3.5 nm of platinum evaporated directly on YAG, shown in Fig. 4.11, exhibits no anomalous Hall-like signature, indicating, that all of the anomalous Hall-like effect observed (c.f. Fig. 4.10) is caused by YIG/Pt interface, as predicted by the SMR theory framework [15].

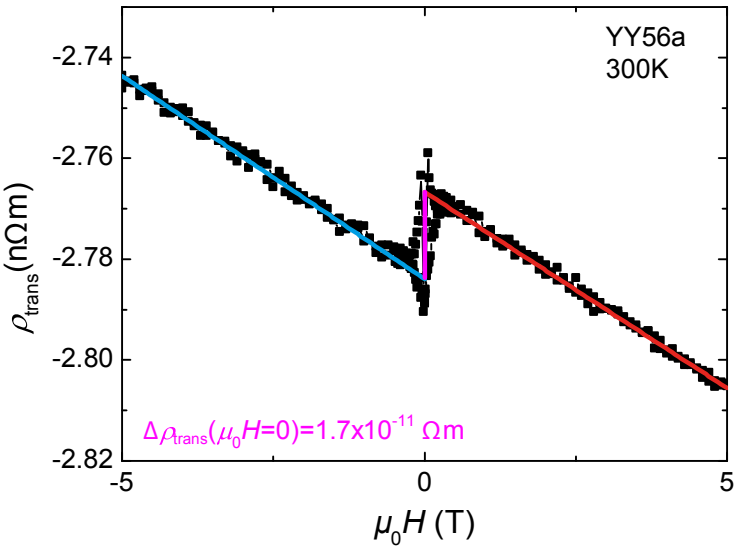

Figure 4.10: Hall measurement of a YIG/Pt hybrid structure in the magnet cryostat. One can obtain the anomalous Hall contribution by interpolating both fitted curves (red and cyan lines) back to $\mu_0 H = 0\,\mathrm{T}$ and taking the differences of the abscissae (magenta line).

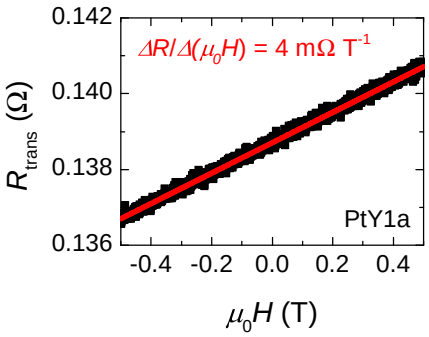

Figure 4.11: Hall measurement of a hybrid structure with platinum ($t_{\mathrm{Pt}} = 3.5\,\mathrm{nm}$) evaporated directly on the substrate YAG. The anomalous Hall-like signature shown in Fig. 4.10 is not visible in this plot, so no anomalous Hall effect is present.

In Fig. 4.12 the resulting contributions of the anomalous Hall effect to the specific resistance is plotted against the thickness of the platinum film. The data recorded at 300 K are shown as black squares, the data for 100 K as red circles and the data measured at 10 K are depicted as blue triangles. The black curve shown in Fig. 4.12 represents Eq. (2.10) with the parameters extracted by Althammer *et al.* [13] at $T = 300\,\mathrm{K}$ and Eq. (4.9) shown in Sec. 4.2 with the fitted parameters. The blue and orange dashed lines represent the same theory curve, using two different sets

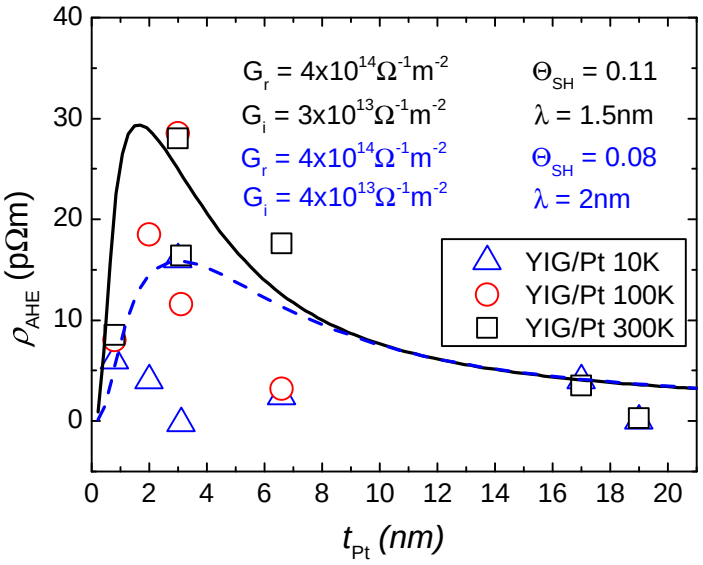

Figure 4.12: Measured contribution of the anomalous Hall effect to the transverse specific resistance plotted against the thickness t_{Pt} of the platinum film. The black line is the expected signal for spin Hall anomalous Hall effect (c.f. Sec. 2.5. The blue dashed lines represents the same curve with different parameters to match the data measured at 10 K.

of parameters to reproduce the trend of the data measured at 10 K. The opposite sign compared to Fig. 2.6 is due to the opposite orientation of the Hall bar in the magnetic field ($\mathbf{n} \uparrow\downarrow \mathbf{H}$ and not $\mathbf{n} \uparrow\uparrow \mathbf{H}$).

The curve coincides with the measured data at $T = 300\,\mathrm{K}$, although the variance of the data is high. Furthermore, more hybrid structures need to be investigated in the regime of $3\,\mathrm{nm} < t_{\mathrm{Pt}} < 6\,\mathrm{nm}$ to probe the theory's predictions.

As the trend is not clearly visible for lower temperatures, different values were used to reproduce the data. The blue curve features a slightly increased imaginary part of the spin mixing interface conductance G_{i} and spin diffusion length λ. As the mean free path in a normal metal increases with decreasing temperature [25], the spin diffusion length should also increase for lower temperatures. It looks like this is the case, as the maximum of the curve shifts to slightly higher platinum thicknesses. The curve just represents an approach to the data measured at 10 K, as it does not sufficiently explain the measured data. The increase of the spin diffusion length is contrary to the observations in the longitudinal SMR effect [29].

One can also obtain the anomalous Hall effect's contribution by measuring the transverse specific resistance during rotations of the YIG/Pt hybrid structures within a fixed magnetic field. For this, the sample needs to be mounted in an out of plane geometry as described in the previous section. Additionally, the ordinary Hall coefficient A_{OHE} needs to be known for the given metal. One then has

$$\rho_{\mathrm{AHE}} = \rho_{\mathrm{trans}} - A_{\mathrm{OHE}}\mu_0 H \tag{4.14}$$

The rotations of the hybrid structures within a fixed magnetic field were carried out in a magnet cryostat at $\mu_0 H = 1\,\mathrm{T}$ ensuring parallel alignment of the magnetization with the external field ($\mathbf{H} \parallel \mathbf{M}_{\mathrm{YIG}}$), as $\mu_0 H \gg \mu_0 H_{\mathrm{sat}} \approx 200\,\mathrm{mT}$.

Additionally, the temperature was adjusted to different constant levels from $T = 10\,\mathrm{K}$ to $T = 300\,\mathrm{K}$ without remounting or reconnecting the samples inbetween measurements. From the obtained transverse voltages the transverse specific resistance was calculated using

$$\rho_{\mathrm{trans}} = \frac{V_{\mathrm{trans}}}{I} t_{\mathrm{Pt}}, \tag{4.15}$$

where I is the driving current along the Hall bar direction $\mathbf{j}$.

After obtaining the specific resistances, the data were antisymmetrized around $\beta = 180°$. The definition of the angle can be seen in the inset of Fig. 4.13. The (anti-)symmetrization splits the signal into two components, one that only inherits symmetric components

$$\rho^{\mathrm{sym}}_{\mathrm{trans}}(\beta) = \rho^{\mathrm{sym}}_{\mathrm{trans}}(\beta + 180°), \tag{4.16}$$

e.g. $\rho_{\text{trans}}^{\text{sym}} = \cos^2(\beta)$, and one that only inherits antisymmetric components

$$\rho_{\text{trans}}^{\text{antisym}}(\beta) = -\rho_{\text{trans}}^{\text{antisym}}(\beta + 180°), \tag{4.17}$$

e.g. $\rho_{\text{trans}}^{\text{antisym}} = \sin(\beta)$.

This was done, as, for slight misalignments of the Hall bar contacts in longitudinal direction, the longitudinal signal, having a $\cos^2(\beta)$ shape due to the longitudinal SMR, is superimposed on the transverse signal. By antisymmetrizing, one can eliminate the $\cos^2(\beta)$ term as it is 180°-symmetric, whereas the $\sin(\beta)$ term of the Hall effect is 180°-antisymmetric. The outcome of such a symmetrization process can be seen in Fig. A.2.

The rotations of the hybrid structures within a fixed magnetic field were performed in two rotation directions, so utilizing the data obtained from both, the clockwise and counterclockwise rotations of the hybrids structures in a fixed magnetic field, allows to obtain one (anti-)symmetrized 360° dataset. One can formulate

$$\rho_{\text{trans}}^{\text{antisym}}(\beta) = \begin{cases} \dfrac{\rho_{\text{trans},1}(\beta) - \rho_{\text{trans},2}(\beta + 180°)}{2} & \text{for } \beta \leq 180° \\ \dfrac{\rho_{\text{trans},1}(\beta) - \rho_{\text{trans},2}(\beta - 180°)}{2} & \text{for } \beta > 180° \end{cases} \tag{4.18}$$

to achieve the symmetrization, where $\rho_{\text{trans},1}(\rho_{\text{trans},2})$ denotes the measured transverse specific resistance while rotating from $\beta = 0°(360°)$ to $\beta = 360°(0°)$. The symmetric part of the specific resistance is obtained by adding the terms in the fractions and not subtracting them.

Figure 4.13 shows the measured transverse specific resistance during the rotation of a hybrid structure with $t_{\text{Pt}} = 8.5\,\text{nm}$ within a fixed magnetic field of $\mu_0 H = 1\,\text{T}$. The transverse specific resistance is modulated by a $\sin(\beta)$ as expected for the Hall effect (c.f. Eq. (2.6)). As the structure was measured at several temperatures, the temperature dependence of the transverse specific resistance can be identified. For an increas of temperature, the specific resistance increases. It was recently observed, that the spin Hall angle increases with increasing temperature [29]. So, assuming all temperature dependence is due to the spin Hall AHE, the change of the specific resistance is quantitatively explained.

Figure 4.14 displays the measured transverse specific resistance while rotating a hybrid structure with $t_{\text{Pt}} = 2.0\,\text{nm}$ in a fixed magnetic field of $\mu_0 H = 1\,\text{T}$. The signal shows the expected behaviour for $T = 300\,\text{K}$, but changes its sign for temperatures lower than $T < 250\,\text{K}$. This sign change was reproduced in several hybrid structures with low platinum thicknesses and is not expected. The shape of the signal for very low temperatures seems to include a higher order term anitsymmetric within 180°, like a $\sin^3(\beta)$. From a fit to the data, using $\rho_{\text{trans}}(\beta) = a\sin(\beta) + b\sin^3(\beta)$, a relative intensity of $\frac{a}{b} = -2.8$ was obtained. This might indicate additional effects,

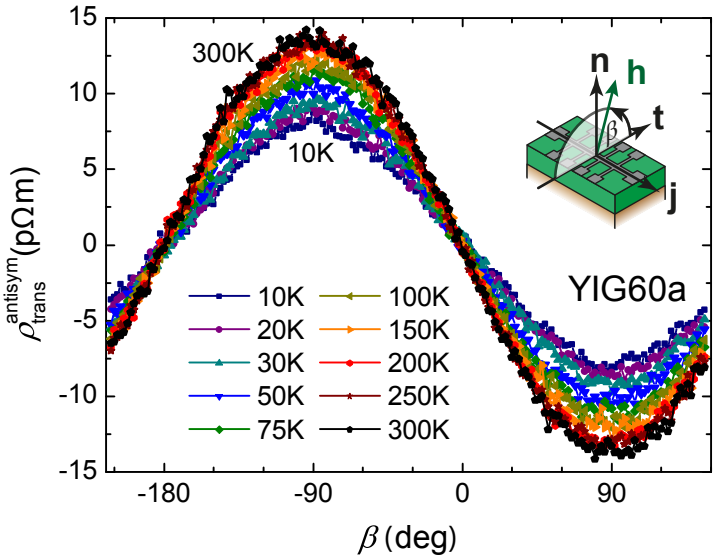

Figure 4.13: Temperature dependent measurements of the transverse specific resistance of a YIG/Pt hybrid structure with $t_{\mathrm{Pt}} = 8.5\,\mathrm{nm}$ mounted in out of plane geometry and rotated around the **j**-axis (oopj) at $\mu_0 H = 1\,\mathrm{T}$.

unaccounted for by the (second order) SMR theory framework up to now [15]. It should be noted, that, also for other samples with thin platinum layers, the $\sin^3(\beta)$ term has the same order of magnitude as the $\sin(\beta)$ term.

The transverse specific resistance is made up of the contributions of ordinary and anomalous Hall effect ($\rho_{\mathrm{trans}} = A_{\mathrm{OHE}} B + \rho_{\mathrm{SHAHE}}$). Therefore, the sign change originates from the change of the ordinary Hall coefficient for very low platinum thicknesses, as the anomalous Hall effect's contribution is positive (c.f. Fig. 4.12).

In Fig. 4.15(upper panel) the raw data measured during an angle dependent measurement of the transverse specific resistance is shown. The shape of the signal is not a $\sin(\beta)$ as expected for a rotation in Hall geometry (c.f. insert in Fig. 4.14). Therefore the symmetrization was carried out. As there is a portion of the longitudinal signal ρ_{long} superimposed on to the transverse signal ρ_{trans} due to small misalignments of the Hall bar contacts, first the crosstalk has to be estimated, which is done, by dividing the transverse signal by the longitudinal signal

$$\max\left(\rho_{\mathrm{trans}}/\rho_{\mathrm{long}}\right) \approx 1\%\,. \tag{4.19}$$

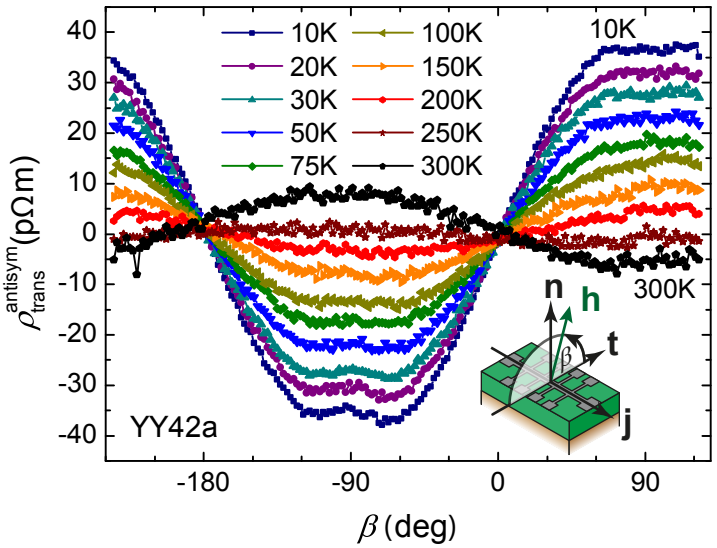

Figure 4.14: Temperature dependent measurement of the transverse specific resistance of a YIG/Pt hybrid structure with $t_{Pt} = 2.0\,\text{nm}$ mounted in out of plane geometry and rotated around the **j**-axis (oopj) at $\mu_0 H = 1\,\text{T}$.

This crosstalk can now be subtracted from the transverse signal

$$\rho_{\text{trans,adjusted}} = \rho_{\text{trans}} - \max\left(\frac{\rho_{\text{trans}}}{\rho_{\text{long}}}\right)\rho_{\text{long}}. \tag{4.20}$$

After symmetrization of the adjusted raw data $\rho_{\text{trans,adjusted}}$, an additional term observed in the antisymmetric component of the angle dependent measurements of the specific resistance. Therefore, the symmetric portion of the signal was analyzed for one sample. The result of this part of the transverse signal is shown in the lowest panel in Fig. 4.15 and is not a straight line, as one would expect, if all transverse symmetric signal is due to the superimposed longitudinal signal. This suprising symmetric signal, which is at least 1/2 of the antisymmetric signal, was only recently discovered and should be topic of further investigations.

As the ordinary Hall coefficient is now known, a quantitative analysis of the angle dependent measurements of the specific resistance was carried out. The connection between the angle dependent measurements and the Hall measurements carried out at $\beta = -90°$ is given by

$$\rho_{\text{trans}} = \rho_{\text{trans,SHAHE}} + A_{\text{OHE}}\mu_0 H. \tag{4.21}$$

Thus, to compare both sets of data, the transverse specific resistance at $\beta = -90°$

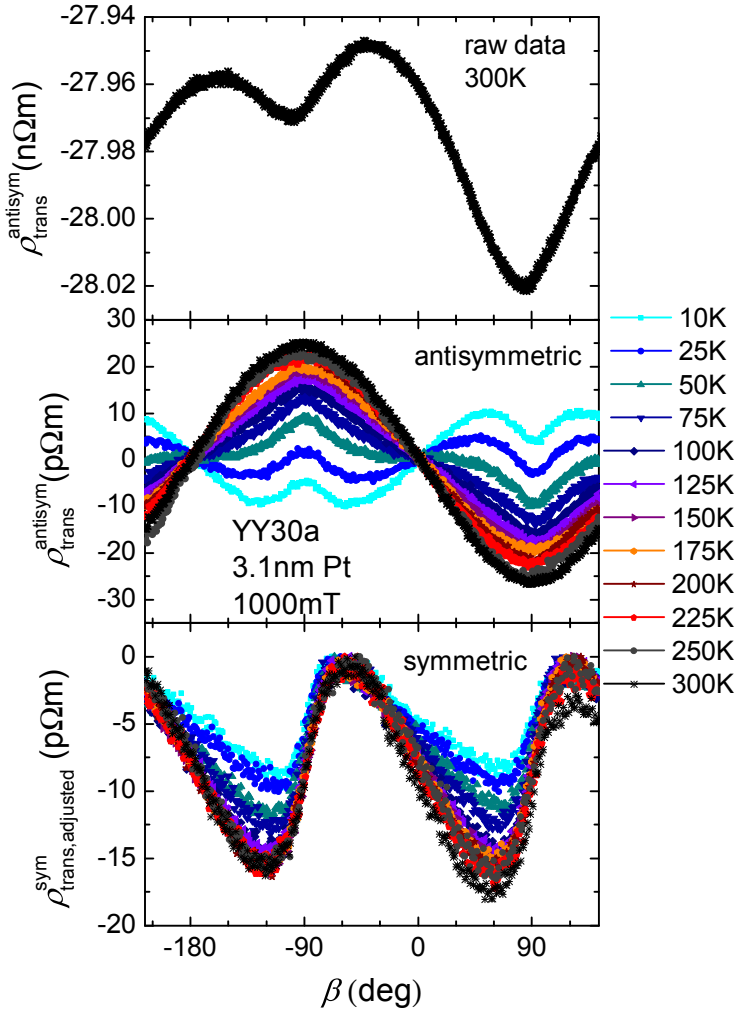

Figure 4.15: Comparison of the temperature dependence of the antisymmetrized and symmetrized data. As the raw data obtained by the magnet cryostat system during an angle dependent measurement of the transverse specific resistance is superimposed by the longitudinal signal (c.f. Fig. A.2), the symmetization was carried out. To obtain the symmetric part of the transversal signal, the crosstalk $\rho^{sym}_{trans}/\rho^{sym}_{long} \approx 1‰$ has to be subtracted from the signal. This was done for the data shown in the lowest panel. It is clearly visible, that the transversal data inherit a symmetric component.

($\mathbf{H} \nparallel \mathbf{n}$) is plotted against the thickness of the platinum film in Figure 4.16. The dashed purple line represents the ordinary Hall effect's contribution to the transverse specific resistance at $\mu_0 H = 1\,\mathrm{T}$. For hybrid structures with $t_{\mathrm{Pt}} > 6\,\mathrm{nm}$ the ordinary Hall effect fully explains the measured data. This is expected, as the spin

Hall anomalous Hall effect decreases with increasing thickness. For thinner films, the experimental data can not be explained by the OHE alone. However, if both contributions (ordinary and extraordinary Hall effect) are taken into account, the data can be explained by Eq. (4.21) $T = 300\,\mathrm{K}$.

For lower temperatures, however, the measurements of the angle dependent transverse specific resistance are not reflected by the two terms in Eq. (4.21). The disagreement can be explained by the additional symmetric term, that has been neglected in Fig. 4.16, as it has the same order of magnitude as the antisymmetric signal.

In summary, it can be concluded, that both measurements techniques, the field sweeps and the angular rotations, are equivalent for a temperature of 300 K, thus it is possible to extract the anomalous Hall effect's contribution from a rotation at $\mu_0 H = 1\,\mathrm{T}$, if the ordinary Hall coefficient is known. The experimental efforts described in Sec. 4.3 to determine $A_{\mathrm{OHE}}(t_{\mathrm{Pt}})$ thus enable this experimental procedure.

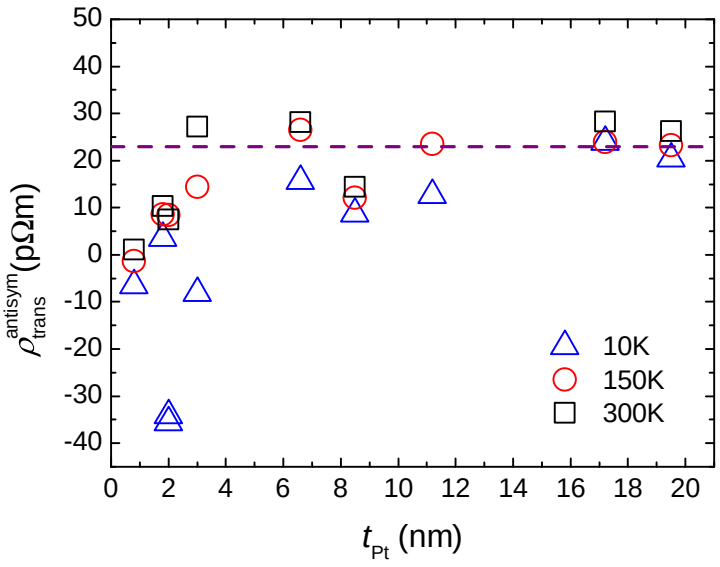

Figure 4.16: Measured maximal transverse specific resistance taken from rotations at a constant external magnetic field plotted against the thickness of the platinum thin film at three different temperatures. The dashed line shows the contribution of the ordinary Hall effect (OHE) at $\mu_0 H = 1\,\mathrm{T}$ [38].

Chapter 5

Conclusions and Outlook

This thesis focussed on probing the predictions made by the spin Hall magnetoresistance (SMR) theory framework related to the transverse specific resistance of YIG/Pt hybrid structures and measuring the ordinary Hall coefficient for very thin platinum films. The results of these measurements will shortly be summarized in this chapter and some suggestions about future experiments will be given.

Within this thesis we reported on substantial changes of the ordinary Hall coefficient A_{OHE} of platinum films for very low thicknesses $t_{\mathrm{Pt}} < 3\,\mathrm{nm}$ (c.f. Sec. 4.3). These effects might originate from finite size effects, as it was previously observed for thin gold films [40]. Furthermore, these finite size effects should increase for lower temperatures, as the mean free path of the electrons is increased compared to room temperature [25].

To probe this, one would need to estimate the predictions made by the Fuchs-Sondheimer theory [34, 35] for the Hall mobility μ_{Hall} (and therefore for A_{OHE}) of thin platinum films, which was not done here due to time constraints.

If the thickness dependence of the ordinary Hall effect is explained by the Fuchs-Sondheimer theory, this effect might come in handy to determine the thickness of very thin platinum films, as the ordinary Hall coefficient can easily be determined by magnetic field sweeps using a magnet setup. This is especially helpful, if the platinum film thickness is so low, that it is hard to distinguish from its underlaying material in a reflectometry measurement. It might even enable one, to estimate the thickness of a platinum film between two layers of another material (e.g. a YIG/Pt/YIG trilayer [14]).

Currently, it seems, that the change of the ordinary Hall coefficient is independent of the YIG film, as the reference samples with platinum grown directly on the substrate (yttrium aluminum garnet, YAG) also displays the change of the ordinary Hall coefficient (c.f. Fig. 4.4). This will need to be verified, as only two samples were analyzed yet.

Furthermore, an anomalous Hall-like effect was observed in YIG/Pt hybrid structures, but not in platinum films evaporated directly on YAG (c.f. Sec. 4.4). As

the magnetic stray field of the YIG's magnetization is one possible reason for the anomalous Hall effect, calculations for the demagnetization field within the YIG thin films were made (c.f. Sec. 4.1).

These calculations show, that in out of plane geometry (where the magnetization vector points perpendicular to the film plane), roughly 99 % of the YIG's magnetization is compensated by the demagnetization field. Thus, there is no significant increase of the magnetic field within the platinum film, that could explain the anomalous Hall effect.

The SMR theory framework predicts an anomalous Hall-like effect for YIG/Pt hybrid structures. This predicted effect, resulting from the imaginary part of the spin mixing interface conductance $G_{\uparrow\downarrow}$ (c.f. Sec. 2.5), sufficiently explains the data measured at 300 K and thus, is verified by a second experimental effort. Therefore, another step to prove the SMR theory framework, also successful in explaining the measurements for the longitudinal signal carried out by Nakayama *et al.* [12] and Althammer *et al.* [13], has been made. However, the low temperature data of the measurements for the anomalous Hall effect indicate an increase of the spin diffusion length λ for low temperatures, contradicting the measurements of the longitudinal SMR [29].

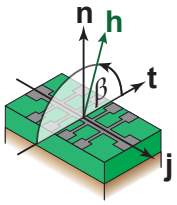

Figure 5.1: Definition of the coordinate system for out of plane rotations of the magnetic field around **j**.
In analogy to [13].

The angle β dependent measurements (c.f. Fig. 5.1) of the transverse specific resistance within a fixed magnetic field however, are difficult to explain for lower temperatures. One would assume to see a $\sin(\beta)$ term due to the ordinary Hall effect (OHE, c.f. Sec. 2.4) and the spin Hall anomalous Hall effect (SHAHE, c.f. Sec. 2.5) for this rotation geometry. Therefore the angle dependence of the transverse specific resistance can be written as (assuming the magnetization of the YIG film is saturated)

$$\rho_{\mathrm{trans}}(\beta) = (\rho_{\mathrm{SHAHE}} + \rho_{\mathrm{OHE}}) \sin(\beta). \tag{5.1}$$

This is exactly what is observed at room temperature and for high platinum thicknesses. However, higher order terms ($\sin^n(\beta)$ with $n \geq 2$, c.f. Fig. 4.14) come into play at lower temperatures and small platinum thicknesses. This might be the reason for the strong temperature dependence of the ordinary Hall coefficient observed in the cryostat (c.f. Sec. 4.3), since one can't distinguish between a $\sin(\beta)$ or $\sin^3(\beta)$

like dependence in the field sweeps at $\beta = -90°$ (**H** perpendicular to the film plane). These higher order terms, currently unaccounted for by theory, result from unknown physics and should be subject to further investigations.

To seperate the higher order terms from the expected $\sin(\beta)$ term, additional work has to be done in explaining the temperature dependence of the ordinary and the anomalous Hall-like effect. If the $\sin(\beta)$ term is well understood, it can be subtracted from the signal, allowing to analyze the additional terms more accurately. From fits to the data, using a $\sin^3(\beta)$ term, it can be estimated, that the higher order terms have approximately the same magnitude as the $\sin(\beta)$ term for very thin platinum films and low temperatures $T = 10\,\mathrm{K}$. This is easpecially interesting, as the additional terms were observed during rotations at room temperature.

To probe the source of the higher order terms, a different material with low spin orbit coupling, but a similar Fermi surface could be used. By doing this, it can be tested, whether these effects rely on intrinsic spin effects or the proximity of a ferromagnetic insulator.

Appendix A

Symmetrization with PYTHON

(Anti-)symmetrization is used to split a signal into two components, one component symmetric in the angle $\beta = 180° = \pi$

$$\rho_{\text{trans}}^{\text{sym}}(\beta) = \rho_{\text{trans}}^{\text{sym}}(\beta + 180°), \tag{A.1}$$

and one component antisymmetric in $\beta = 180°$

$$\rho_{\text{trans}}^{\text{antisym}}(\beta) = -\rho_{\text{trans}}^{\text{antisym}}(\beta + 180°). \tag{A.2}$$

Therefore, the angle where the symmetrization is started does not matter, as always another point displaced by $\beta = \pm 180°$ is used. Here, PYTHON was used to (anti-)symmetrize the transverse data obtained during the rotations of the hybrid structures within a magnetic field to seperate the longitudinal portion of signal (which has a $\cos^2(\beta)$ shaped angle dependence and thus is symmetric in $\beta = 180°$) superimposed on the transverse signal (which has a $\sin(\beta)$ dependence on the angle and therefore is antisymmetric in $\beta = 180°$) due to slight misalignments of the leads at the Hall bar. Thus, the symmetrization allows to "cleanse" the transverse data of the longitudinal crosstalk. The equation used to (anti-)symmetrize the data is

$$\rho_{\text{trans}}^{\text{antisym}}(\beta) = \begin{cases} \dfrac{\rho_{\text{trans},1}(\beta) - \rho_{\text{trans},2}(\beta + 180°)}{2} & \text{for } \beta \leq 180°, \\ \dfrac{\rho_{\text{trans},1}(\beta) - \rho_{\text{trans},2}(\beta - 180°)}{2} & \text{for } \beta > 180°, \end{cases} \tag{A.3}$$

where $\rho_{\text{trans},1}(\rho_{\text{trans},2})$ denotes the measured transverse specific resistance while rotating from $\beta = 0°(360°)$ to $\beta = 360°(0°)$. The symmetric part of the specific resistance is obtained by adding the two terms in the fraction instead of subtracting them. The result of such a symmetrization is shown in Fig. A.2.

This was implemented in PYTHON with direct input of data generated by the Labview-program used to control the angle dependent magnetoresistance measurements. The prefix of the files needs to be "admr_". So, by adding a "#" in front the filename, a file can be omitted from the symmetrization (like putting a comment

into a computer program).

The routine can also be used to symmetrize an arbitrary set of angle dependent data:
To achieve this, the data has to be formatted into a plain ascii text file (filename has to contain "simu"), where the first column contains the angle of rotation (integers), the second the longitudinal set of data (floats with points as seperators) and the third the transverse set of data (also floats). The columns have to be seperated by 1 tabulator (this coincides with the ascii-export done by Origin 8.6). The transverse set of data can be ommited, so only the first set is (anti-)symmetrized. The data does not need to be sorted!

To run the (anti-)symmtrization, the path where the files are located and a list containing the filenames of the data files prepared as described above needs to be provided to the routine (not necessary if all files within the path should be used). The format of a list in PYTHON is [file1,file2,...].

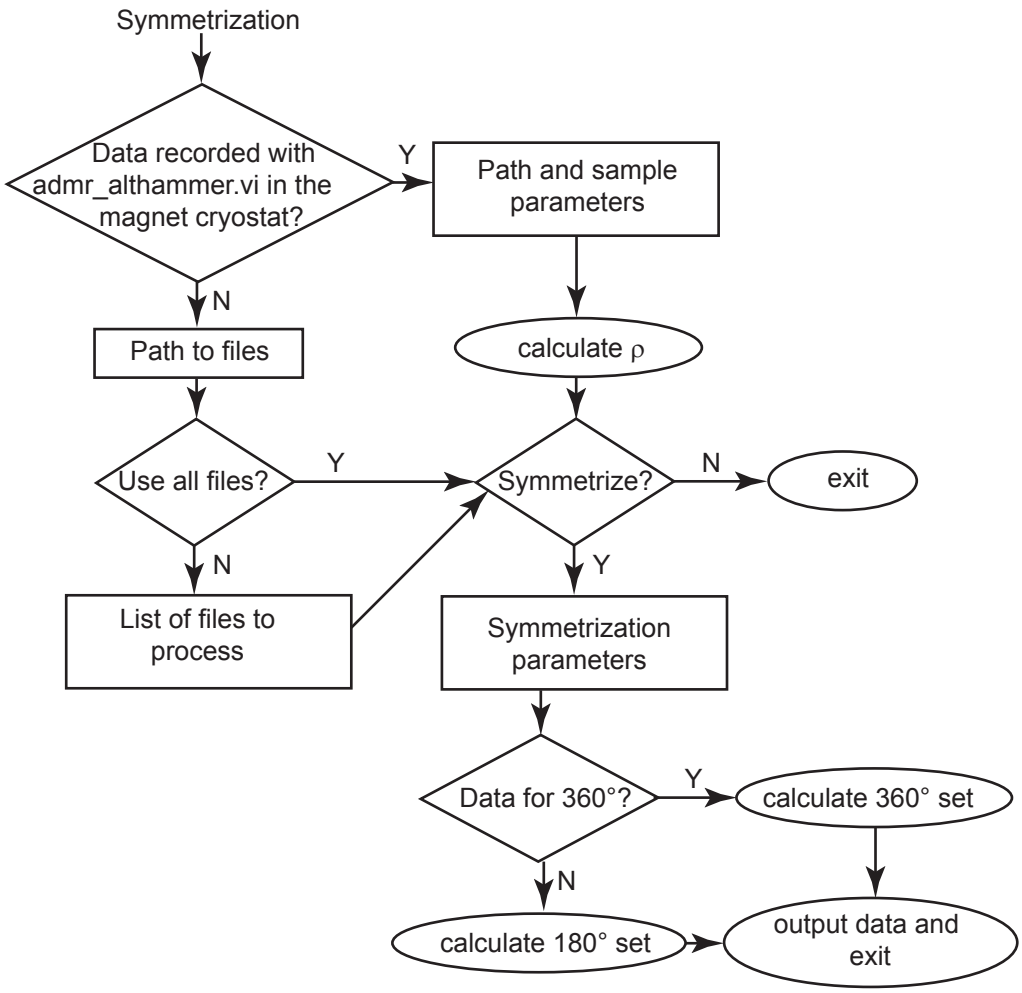

Figure A.1: Block diagram for the usage of the PYTHON routine written during this thesis.

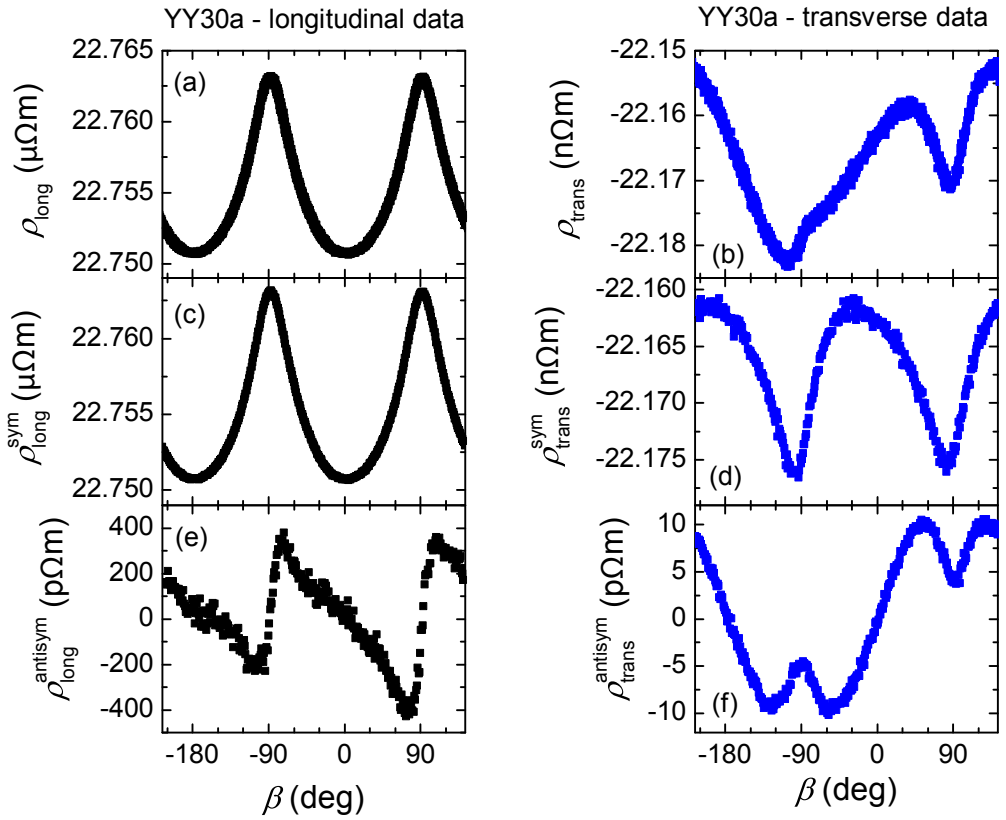

Figure A.2: Example of the symmetrization routine's output. One can clearly see the longitudinal component in (a) superimposed on the transverse signal in the raw data in (b). After symmetrization, these components are seperated ((d) and (f)).

Appendix B

Used Samples

Table B.1: Table containing all samples used during this thesis. The values inside the brackets correspond to the layer thickness in nm. For the layers with a questionmark within the brackets, the layer thickness was unknown.

Sample	layers (thickness in nm)
PtY1	YAG|Pt(3.5)
PtY3	YAG|Pt(15.5)
YY17a	YAG|YIG(64.2)|Pt(3.0)
YY21a	YAG|YIG(61.0)|Pt(19.5)
YY22a	YAG|YIG(63.0)|Pt(6.6)
YY30a	YAG|YIG(55.5)|Pt(3.1)
YY32a	YAG|YIG(57.7)|Pt(2.5)
YY42a	YAG|YIG(?)|Pt(2.0)
YY56a	YAG|YIG(?)|Pt(0.8)
YIG53a	GGG|YIG(53.3)|Pt(2.5)
YIG55a	GGG|YIG(46.2)|Pt(3.5)
YIG56a	GGG|YIG(68.7)|Pt(2.7)
YIG59a	GGG|YIG(60.7)|Pt(11.2)
YIG60a	GGG|YIG(53.0)|Pt(8.5)
YIG70a	GGG|YIG(54.8)|Pt(17.2)
YIG73a	GGG|YIG(28.9)|Pt(1.8)
YIG105a	GGG|YIG(16.3)|Pt(2.8)
YIG121a	GGG|YIG(?)|Pt(3.0)

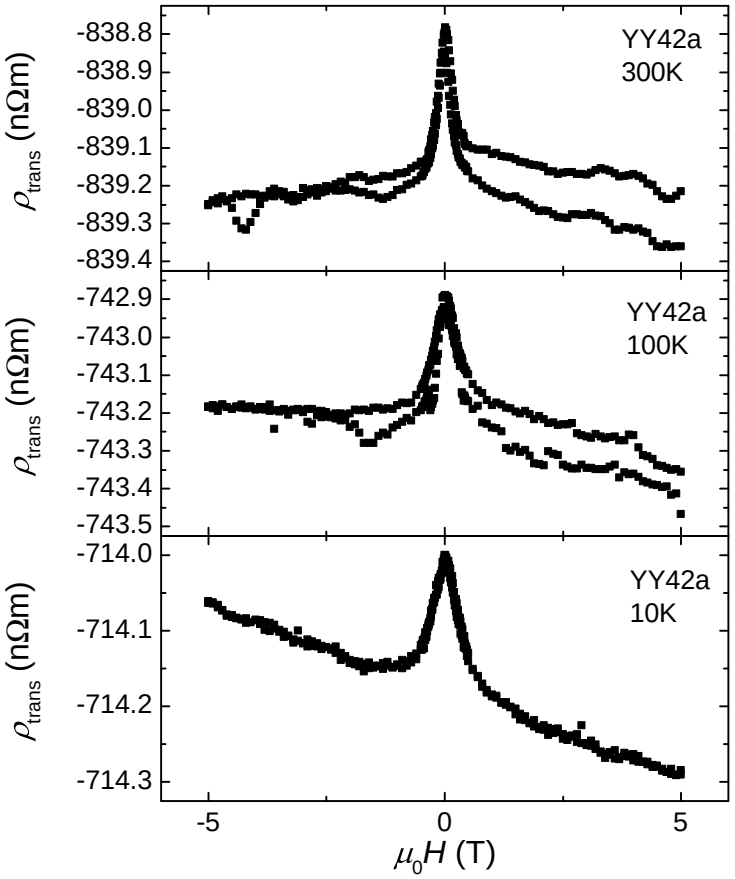

Figure B.1: Hall measurement of the sample YY42 with $t_{\mathrm{Pt}} = 2\,\mathrm{nm}$. The slopes of the saturation regime for 300 K and 100 K (upper panels) are hard to determine

Bibliography

[1] E. H. Hall. On a New Action of the Magnet on Electric Currents. *American Journal of Mathematics* **2**, pp. 287–292 (1879). URL.

[2] E. H. Hall. XVIII. On the "Rotational Coefficient" in nickel and cobalt. *Philosophical Magazine Series 5* **12**, 157–172 (1881). URL.

[3] R. Karplus & J. M. Luttinger. Hall Effect in Ferromagnetics. *Physical Review* **95**, 1154–1160 (1954). URL.

[4] M. V. Berry. Quantal Phase Factors Accompanying Adiabatic Changes. *Proceedings of the Royal Society of London. A. Mathematical and Physical Sciences* **392**, 45–57 (1984). URL.

[5] N. Nagaosa, J. Sinova, S. Onoda, A. H. MacDonald & N. P. Ong. Anomalous Hall effect. *Reviews of Modern Physics* **82**, 1539–1592 (2010). URL.

[6] S. Geprägs, S. Meyer, S. Altmannshofer, M. Opel, F. Wilhelm, A. Rogalev, R. Gross & S. T. B. Goennenwein. Investigation of induced Pt magnetic polarization in $Pt/Y_3Fe_5O_{12}$ bilayers. *Applied Physics Letters* **101**, 262407 (2012). URL.

[7] J. E. Hirsch. Spin Hall Effect. *Physical Review Letters* **83**, 1834–1837 (1999). URL.

[8] S. Murakami, N. Nagaosa & S.-C. Zhang. Dissipationless Quantum Spin Current at Room Temperature. *Science* **301**, 1348–1351 (2003). URL.

[9] Y. K. Kato, R. C. Myers, A. C. Gossard & D. D. Awschalom. Observation of the Spin Hall Effect in Semiconductors. *Science* **306**, 1910–1913 (2004). URL.

[10] S. O. Valenzuela & M. Tinkham. Direct electronic measurement of the spin Hall effect. *Nature* **442**, 5 (2006). URL.

[11] E. Saitoh, M. Ueda, H. Miyajima & G. Tatara. Conversion of spin current into charge current at room temperature: Inverse spin-Hall effect. *Applied Physics Letters* **88**, 182509–182509–3 (2006). URL.

[12] H. Nakayama, M. Althammer, Y.-T. Chen, K. Uchida, Y. Kajiwara, D. Kikuchi, T. Ohtani, S. Geprägs, M. Opel, S. Takahashi, R. Gross, G. E. W. Bauer, S. T. B. Goennenwein & E. Saitoh. Spin Hall Magnetoresistance Induced by a Nonequilibrium Proximity Effect. *Physical Review Letters* **110**, 206601 (2013). URL.

[13] M. Althammer, S. Meyer, H. Nakayama, M. Schreier, S. Altmannshofer, M. Weiler, H. Huebl, S. Geprägs, M. Opel, R. Gross, D. Meier, C. Klewe, T. Kuschel, J.-M. Schmalhorst, G. Reiss, L. Shen, A. Gupta, Y.-T. Chen, G. E. W. Bauer, E. Saitoh & S. T. B. Goennenwein. Quantitative study of the spin Hall magnetoresistance in ferromagnetic insulator/normal metal hybrids. *Physical Review B* **87**, 224401 (2013). URL.

[14] D. Irber. *Spin Hall Magnetoresistance in F/N/F trilayers.* Bachelor's thesis, Technische Universität München (2013).

[15] Y.-T. Chen, S. Takahashi, H. Nakayama, M. Althammer, S. T. B. Goennenwein, E. Saitoh & G. E. W. Bauer. Theory of spin Hall magnetoresistance. *Physical Review B* **87**, 144411 (2013). URL.

[16] W. Gerlach & O. Stern. Das magnetische Moment des Silberatoms. *Zeitschrift für Physik* **9**, 353–355 (1922). URL.

[17] F. D. Czeschka. *Spin Currents in Metallic Nanostructures.* Ph.D. thesis, Technische Universität München (2011).

[18] L. Berger. Side-Jump Mechanism for the Hall Effect of Ferromagnets. *Physical Review B* **2**, 4559–4566 (1970). URL.

[19] J. Smit. The spontaneous hall effect in ferromagnetics {II}. *Physica* **24**, 39 – 51 (1958). URL.

[20] M. I. Dyakonov & V. I. Perel. Possibility of Orienting Electron Spins with Current. *Journal of Experimental and Theoretical Physics Letters* **13** (1971).

[21] S. Takahashi & S. Maekawa. Spin current, spin accumulation and spin Hall effect. *Science and Technology of Advanced Materials* **9**, 014105 (2008). URL.

[22] G. Mihajlović, J. E. Pearson, M. A. Garcia, S. D. Bader & A. Hoffmann. Negative Nonlocal Resistance in Mesoscopic Gold Hall Bars: Absence of the Giant Spin Hall Effect. *Physical Review Letters* **103**, 166601 (2009). URL.

[23] F. P. Witek. *Spin Hall Magnetoresistance Noise.* Master's thesis, Technische Universität München (2013).

[24] A. Brataas, Y. Nazarov & G. Bauer. Spin-transport in multi-terminal normal metal-ferromagnet systems with non-collinear magnetizations. *The European Physical Journal B - Condensed Matter and Complex Systems* **22**, 99–110 (2001). URL.

[25] R. Gross & A. Marx. *Festkörperphysik* (Oldenbourg Wissenschaftsverlag, 2012).

[26] F. Schade. *Fabrication and Characterization of $Y_3Fe_5O_{12}/Pt/Y_3Fe_5O_{12}$ Trilayers for Spin Current Based Experiments.* Bachelor's thesis, Technische Universität München (2013).

[27] S. Meyer. *Magneto-thermogalvanische Experimente an (Ga,Mn)As Dünnfilmen.* Diploma thesis, Ludwig-Maximilian-Universität München (2012).

[28] Keithley Instruments, Inc. *Models 2182 and 2182A Nanovoltmeter User's Manual, Rev. A* (2004).

[29] S. Meyer, M. Althammer, S. Geprägs, M. Opel, R. Gross & S. T. B. Goennenwein. Spin Transport Properties of Platinum From Spin Hall Magnetoresistance Measurements. *to be published* (2013).

[30] A. Smith, K. K. Nielsen, D. V. Christensen, C. R. H. Bahl, R. Bjork & J. Hattel. The demagnetizing field of a nonuniform rectangular prism. *Journal of Applied Physics* **107**, 103910 (2010). URL.

[31] A. Aharoni. Demagnetizing factors for rectangular ferromagnetic prisms. *Journal of Applied Physics* **83**, 3432–3434 (1998). URL.

[32] C. Gerthsen, H. O. Kneser & H. Vogel. *Physik* (Springer, 1992), sixteenth edn.

[33] S. Y. Huang, X. Fan, D. Qu, Y. P. Chen, W. G. Wang, J. Wu, T. Y. Chen, J. Q. Xiao & C. L. Chien. Transport Magnetic Proximity Effects in Platinum. *Physical Review Letters* **109**, 107204 (2012). URL.

[34] G. Fischer, H. Hoffmann & J. Vancea. Mean free path and density of conductance electrons in platinum determined by the size effect in extremely thin films. *Physical Review B* **22**, 6065–6073 (1980). URL.

[35] E. H. Sondheimer. The mean free path of electrons in metals. *Advances in Physics* **1**, 1–42 (1952). URL.

[36] N. Vlietstra, J. Shan, V. Castel, J. Ben Youssef, G. E. W. Bauer & B. J. van Wees. Exchange magnetic field torques in YIG/Pt bilayers observed by the spin-Hall magnetoresistance. *ArXiv e-prints* **1305.3117** (2013). URL.

[37] D. Greig & D. Livesey. The Hall coefficient of dilute palladium and platinum alloys. *Journal of Physics F: Metal Physics* **2**, 699 (1972). URL.

[38] C. Hurd. *The Hall Effect in Metals and Alloys.* International Congresses of Quantum Chemistry Series (Plenum Press, 1972).

[39] W. Martienssen & H. Warlimont. *Springer Handbook of Condensed Matter and Materials Data* (Springer, 2005).

[40] R. Henriquez, S. Oyarzun, M. Flores, M. A. Suarez, L. Moraga, G. Kremer, C. A. Gonzalez-Fuentes, M. Robles & R. C. Munoz. Size effects on the Hall constant in thin gold films. *Journal of Applied Physics* **108**, 123704 (2010). URL.

Acknowledgements

I would like to thank the following people for supporting this work:

- Prof. Rudolph Gross, for enabling me to do my bachelor's thesis at the Walther Meißner Institut.
- Dr. Sebastian T. B. Goennenwein, for relentlessly pushing me forward and never stopping to ask questions, while otherwise providing some of the answers to the central questions of this work. Without his input, the explanation of the data would have been much harder.
- Dr. Stephan Geprägs and Dr. Matthias Opel, for taking care of the growth apparatus and the good quality of the samples and for providing their input, when I was stuck with explaining the experimental data during the several Hall-meetings.
- Sibylle Meyer, for always having an open ear for my questions, however stupid they seemed to be. Furthermore, for proofreading this thesis several times, and for always coming in on the weekend, taking care of the cryostat and supporting the whole process of writing this thesis with her creative and clever input. Additionally, for having several lively discussions about the topics investigated, providing much needed input to form the concepts of this thesis. And at last, for growing most of the samples measured during this thesis.
- Dominik Irber, for making the time go by faster, by providing his companionship. Additionally, for providing his help in understanding the topic, mutually expanding each others knowledge.
- Mark Schneider, for providing me with some of the samples measured during this thesis.
- Friedrich Witek, for supporting me with LaTeX-related questions, and for widening my understanding of the SMR, especially in the beginning of my time at the Walther Meißner Institut.
- The staff of the Walther Meißner Institut, for keeping everything running and clean.

- All other fellow people at the Walther Meißner Institut, not addressed yet, for providing such a nice and focussed working environment.